

# Liquid air energy storage (LAES) integrated into the hydrogen economy – Techno-economic optimization of waste cold recovery from liquid hydrogen regasification

Alessio Tafone<sup>1\*</sup>, Roberto Pili<sup>2</sup>, Tobias Massier<sup>1</sup>, Lizhong Yang<sup>3</sup>, Harald Klein<sup>4</sup>

<sup>1</sup> TUMCREATE, 1 CREATE Way, #10-02 CREATE Tower, Singapore 138602


<sup>2</sup> Department of Mechanical Engineering, Section of Thermal Energy, Technical University of Denmark, Lyngby, Denmark

<sup>3</sup> School of Mechanical and Aerospace Engineering, Nanyang Technological University, 639798, Singapore

<sup>4</sup> Technical University of Munich, TUM School of Engineering and Design, Department of Energy and Process Engineering, Institute of Plant and Process Technology, 85748 Garching, Germany

\* Corresponding author. Email: [alessio.tafone@tum-create.edu.sg](mailto:alessio.tafone@tum-create.edu.sg)

## Accepted manuscript

[Liquid air energy storage \(LAES\) integrated into the hydrogen economy – Techno-economic optimization of waste cold recovery from liquid hydrogen regasification](#) © 2025 by Alessio Tafone, Roberto Pili, Tobias Massier, Lizhong Yang and Harald Klein is licensed under the [CC BY-NC-ND 4.0](#) licence . The final published version of this article is available at <https://doi.org/10.1016/j.est.2025.117763>.

## Abstract

A liquid air energy storage (LAES) system is a promising Carnot battery configuration capable of efficiently recovering waste heat and cold energy carriers. Among these, liquid hydrogen (LH<sub>2</sub>) regasification presents temperature, which aligns well with the liquid air liquefaction process. While most existing studies focus on integrating LAES with liquid natural gas (LNG) regasification or improving hydrogen liquefaction via liquid air regasification, this work takes a novel approach by enhancing liquid air liquefaction through the utilization of waste cold from LH<sub>2</sub> regasification. Additionally, this study explores an economic innovation—the valorization of clean dry air discharged by LAES, which has not been extensively examined in prior literature. A novel LAES configuration is proposed and subjected to a techno-economic analysis, comparing its performance with a stand-alone LAES system. Results show that the proposed integration increases round-trip efficiency by 15%, reduces the levelized cost of storage by 60%, and achieves a payback period of under 10 years. These findings provide valuable insights for both academia and industry, advancing the development of more efficient and economically viable LAES systems.

## Keywords

Electrical energy storage, Liquid air energy storage (LAES), Carnot battery, Hydrogen, Waste cold recovery, Process integration

## Highlights

- A novel LAES system aiming to efficiently recover the waste cold from liquid hydrogen regasification is investigated.
- Clean dry air commodity is introduced as a novel potential revenue for LAES.
- A comprehensive techno-economic optimization is carried out.
- The novel solution effectively improves the round-trip efficiency by 15 %.
- The levelized cost of storage is significantly decreased by 60 %.

<b>Nomenclature</b>			
$C$	Capacity rate [W/K]	RTE	Round-trip efficiency
$c_p$	Specific heat capacity [kJ/kg K]	SC	Specific consumption
$D$	TES internal diameter [m]	SH	Superheater
$h$	Enthalpy [kJ/kg]	SHM	Sensible heat material
$h_v$	Volumetric heat transfer coefficient [W/m <sup>3</sup> K]	SIC	Specific investment cost [USD/kW <sub>e</sub> ]
$H$	TES height [m]	SP	Size parameter [m]
$k$	Thermal conductivity [W/m K]	TES	Thermal Energy Storage
$L$	Latent heat [kJ/kg]	VR	Volumetric ratio [-]
$\dot{m}$	Mass flow rate [kg/s]	WHR	Waste Heat Recovery
$NTU$	Number of Transfer Units [-]	<i>Subscripts</i>	
$p$	Pressure [bar]	amb	ambient
$T$	Temperature [°C]	BM	Bare Module
$U$	Overall heat transfer coefficient [W/m <sup>2</sup> K]	C	Cold
$W$	Mechanical Power [kW]	ch	charge
<i>Acronyms</i>		Compr	compression
CDA	Clean Dry Air	d	discharge
CRC	Cryogenic Rankine Cycle	e	electric
CT	CryoTurbine	EVA	Evaporator
CTES	Cold Thermal Energy Storage	G	generator
EES	Electrical Energy Storage	H	Hot
ET	Electricity tariff [USD/kWhe]	I	Inverter
HEX	Heat exchanger	iso	isentropic
HGCS	High Grade Cold Storage	M	Motor
HTF	Heat transfer fluid	max	maximum
HGWS	High Grade Warm Storage	min	minimum
LAES	Liquid Air Energy Storage	poly	polytropic
LAS	Liquid Air Storage	s	storage
LCOS	Levelised cost of storage	T	Turbine
LH2	Liquid Hydrogen	wf	working fluid
LNG	Liquefied natural gas	<i>Greek Symbols</i>	
NPV	Net Present Value	$\eta$	Efficiency [-]
PP	Pinch Point	$\varepsilon$	Porosity [-]
RES	Renewable energy systems	$\varepsilon_{HE}$	Effectiveness [-]

## 1. Introduction

A clean energy supply and the expansion of electrification are key drivers in transitioning toward a net-zero emissions energy system [1]. Consequently, electricity—which will serve as the foundation for future net-zero energy networks—is expected to grow from 20% to 50-70% of global final energy consumption by 2050 [1], primarily through low-emission sources like solar and wind power. To support the rising share of renewables and ensure power system flexibility, the fast-evolving global energy mix will require a diverse set of options, including energy storage solutions and hydrogen technologies [2,3].

Pumped hydro storage has traditionally been the dominant large-scale, long-duration energy storage technology due to its low cost, high efficiency, and long lifespan, accounting for 94% of global bulk energy storage capacity [4]. However, its expansion is highly constrained by geographical limitations. Large-scale batteries have emerged as an alternative and are rapidly advancing, yet they still face challenges such as high costs, limited lifespan, and complex

management requirements [5]. Hydrogen and power-to-X technologies are also considered for large-scale, long-duration storage, but their performances remain low [6]. Carnot batteries, also known as thermo-mechanical energy storage, present another promising characteristic for these applications [5] and include Carnot batteries technologies include pumped thermal electricity storage (PTES)[7], compressed air energy storage (CAES) [8] and liquid air energy storage (LAES) [9].

Liquid air energy storage (LAES) has emerged as a promising solution for electrical energy storage, gaining increasing attention due to its potential benefits. By utilizing air as both the storage medium and working fluid, LAES offers a cost-effective, high-energy-density, and environmentally friendly technology, suitable for medium- to large-scale applications without geographical limitations, unlike pumped hydro or compressed air storage systems [10]. As shown in **Fig. 1**, the LAES process involves air liquefaction through a dedicated cryogenic cycle using electricity in the charging phase, storage phase through a liquid air tank, and then liquid air compression and regasification to generate power during discharge. Thermal energy storage (TES) technologies capture the heat from compression and cold energy from evaporation during these stages, enhancing round-trip efficiency. However, a primary challenge in scaling LAES lies in the substantial energy required during the liquefaction phase, where air must be compressed at high pressures to produce an adequate yield of liquid air.

In particular, the recovery processes of the air regasification cold stream and the air compression heat in the charge and discharge phase, respectively, are crucial to obtain acceptable round-trip efficiency values, as demonstrated by Aliaga et al. [11]. Thus, the keys to ensuring the high efficiency of a LAES system are twofold: 1) the recovery, storage and recycling of the high exergetically valuable cold stream (usually  $-180$  to  $-150$  °C); 2) the recovery, storage and recycle of the waste heat from air compression (usually  $180$  to  $300$  °C), despite only a fraction (55 to 80%) of the compression waste heat is needed for the discharging phase [12].

Furthermore, due to its thermo-mechanical nature, the system can also efficiently harness waste heat (to enhance discharging efficiency) and waste cold energy flows (to augment the performance of the liquefaction process) from different industrial processes [10]. Studies have shown that properly utilizing the excess waste cold from liquid air regasification by first storing and then recirculating this highly valuable exergetic flow in the liquefaction plant improves overall energy efficiency. Indeed, Morgan et al. [13] conducted a pilot-scale study on a LAES system, demonstrating that the low round-trip efficiency was primarily due to only 51% of the available waste cold from air regasification being recovered during the charge phase. Sciacovelli et al. [14] investigated a LAES system incorporating a packed bed to recover waste cold from liquid air regasification and found that storing cold thermal energy using quartzite rock packed beds enhances the baseline system's exergy efficiency by approximately 50%. Huttermann and Span [15] analyzed the impact of different storage materials on the efficiency of a packed bed cold storage system used in LAES to recover cold energy from liquid air regasification. Their analysis showed that the packed bed efficiency increases as volumetric heat capacity decreases, with polypropylene and high-density polyethylene being well-suited as storage materials. Ryu et al. [16] proposed a novel LAES system using a combination of sensible and latent heat thermal storage. By storing the cold energy through the low-temperature phase change medium ( $T_{\text{melting}} = -163$  °C), a round-trip efficiency of 60.6 % is achieved. Tafone et al. [17,18] considered applying low-temperature phase change materials (PCMs) to the cold thermal energy storage of LAES, to obtain higher round-trip efficiency values compared to sensible heat material (SHM) solutions. Qu et al. [19] proposed a cascaded packed bed to store cold energy through SHMs in different temperature ranges. It is shown that the cascaded packed bed cryogenic storage scheme is beneficial to improve the stability and energy efficiency of the system (up to 93 %). In their study, She et al. [20] proposed a novel Referred-Standard-Volume (RSV) optimization method to enhance the thermal performance of packed-bed cold thermal energy storage systems used in cryogenic energy storage. By optimizing the bed volume relative to a standard reference, the study

demonstrates improvements in efficiency and storage density. This method provides a new perspective on the design of cryogenic packed beds and contributes to the advancement of cold thermal energy storage technologies.

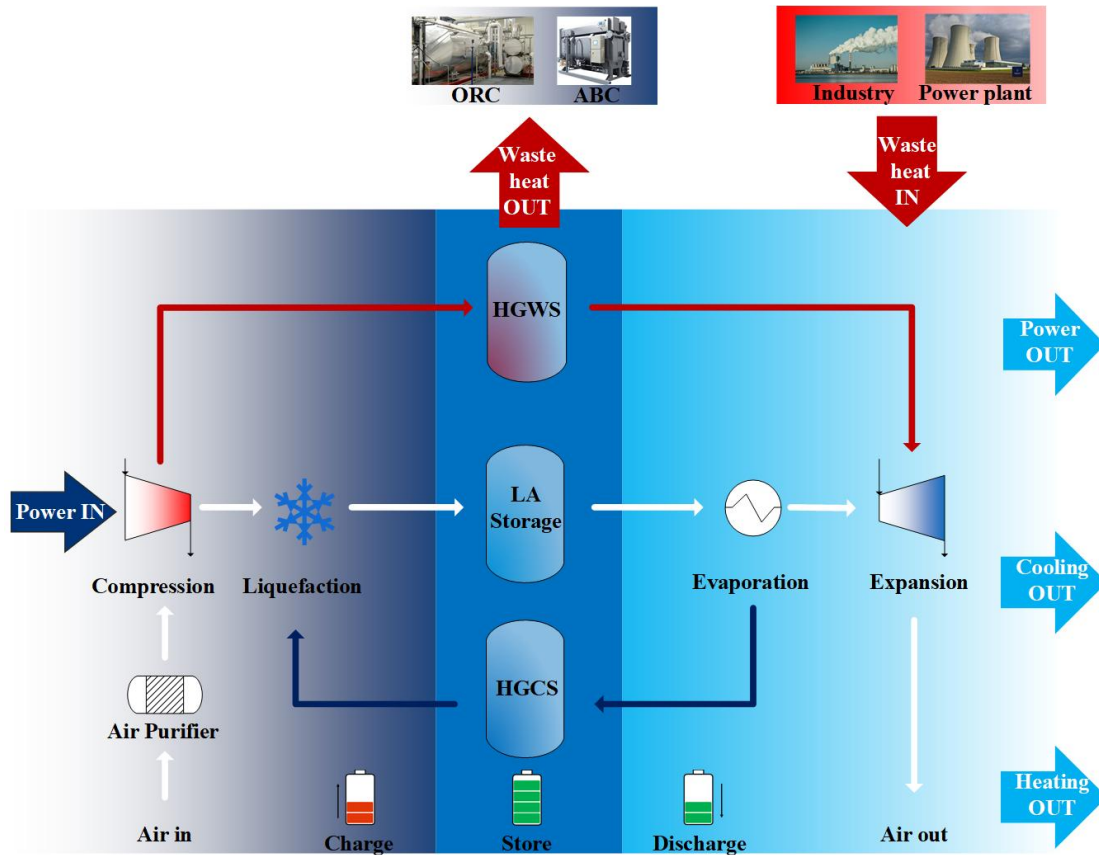


**Fig. 1.** The working principles of a liquid air energy storage (LAES) system integrating different waste heat recovery technologies and external heat sources. Adapted from Ref. [21].

Nevertheless, to partially avoid the investment cost due to the cold thermal energy storage and also to enhance LAES performance, some studies directly used external cold sources for air liquefaction support. The most available cold source in industry in this regard is LNG cold energy. Consequently, the integration of LAES with the LNG regasification process has been extensively studied since 2017 [22] and thereafter a significant amount of literature works has been published. She et al. [23] applied the Brayton cycle for integrating LAES into the LNG regasification system. The core of the authors' system concept was based on the enhancement of the electricity production of the discharge phase using the LNG regasification process as a heat sink for the Brayton cycle. The system integration provides a 56.5 % boost to the round-trip efficiency, achieving values (up to 70.6 %) comparable to other large scale energy storage technologies. Conversely, the same authors [24] investigated the potential of waste cold from LNG regasification to enhance the performance of the air liquefier (i.e. LAES charge phase). The system integration involves the cold thermal energy storage section where the LNG is regasified and subsequently provided to the specific user. The authors observed a more enhanced round-trip efficiency improvement compared to the work of She et al. [23] ( $\eta_{RT} = 78-89\%$  vs  $\eta_{RT} = 70.6\%$ ). A step forward toward the effective integration of the valuable waste cold stream from LNG regasification is provided by the analysis carried out by Park et al. [25]. The authors proposed a LAES-LNG integration model that showed an outstanding round-trip efficiency of 113% and an energy capacity of 0.119 kJ/kg<sub>LNG</sub>. The core of the novelty proposed lies in exploiting the cold

energy recovery for both charge and discharge performance enhancement. The same authors [26] further improved their concept achieving a significantly higher round-trip efficiency of 187.4 %. This was enabled through the effective use of LNG cold energy for air liquefaction and the utilization of organic Rankine cycles (ORC) and direct expansion process, also enabling flexible operation depending on the electricity demand. The related economic analysis suggested that the additional revenue from the regasification service fee provided by the LAES is crucial in the economic viability of the energy storage system, accounting for approximately 82 % of the total revenue.

The above literature review suggests a clear benefit of the integration of the LAES system with the LNG regasification process. However, research on the integration of the liquid hydrogen (LH<sub>2</sub>) regasification process in LAES liquefaction plants is almost absent in the existing literature. One recent work proposed by Kim et al.[27] investigated the techno-economic feasibility of the waste cold integration by liquid hydrogen regasification with LAES. The study highlighted that, depending on the LAES configuration adopted, the round-trip efficiency can be augmented up to 150 % with a net present value of 38.61 MUSD. Overall, hydrogen has become a key cornerstone in the decarbonization scenarios of different countries and worldwide [28]. For instance, aiming at halving its carbon emissions, Singapore has promoted the adoption of different decarbonization strategies among which the adoption of hydrogen as key low-carbon fuel for both power and alternative marine fuels production [29]. Since in the short-medium term large-scale electrolyzer plants face obstacles like high costs, insufficient standards, and restricted space for renewable energy installations—especially on a small tropical island like Singapore—importing green hydrogen emerges as a practical alternative to decrease fossil fuel reliance and reduce carbon emissions [30]. To this end, Keppel infrastructure partnering with Mitsubishi Power Asia Pacific planned to develop the first hydrogen fueled 600 MW<sub>e</sub> cogeneration power plant (Keppel Sakra Cogen Plant) located in Jurong island, Singapore. The initial plan is to co-fire the power plant with a 30 % hydrogen blend by 2026 and progressively reach up to 100 % hydrogen as soon as this energy vector will become a more economically viable solution [31]. This scenario will serve as the foundation for the authors' investigation of LAES integrated with liquid hydrogen regasification. Indeed, considering LH<sub>2</sub> as one of the three most promising technologies for long-distance hydrogen transportation since it is potentially inexpensive, safe, and easily manageable [32], this study evaluates the application of a co-located regasification plant for liquid hydrogen. According to IRENA [30] and Hank et al. [32], the medium-long term scenarios depict liquid hydrogen as the most cost-effective and safest hydrogen carrier. The LH<sub>2</sub> concept (**Fig. 2**) employs a liquefaction process to obtain liquid hydrogen. The product is transported to potential users via LH<sub>2</sub> vessels. During the regasification, LH<sub>2</sub> is vaporised and H<sub>2</sub> is released. As highlighted by Restelli et al. [33], the whole supply chain is highly energy demanding especially during the liquefaction process and can take up to ~80% of the levelized cost of the whole process for both present and future scenarios. As a result, efficiently utilizing the waste cold released during the regasification phase could be a game changer, significantly enhancing the overall efficiency of the entire supply chain.

Furthermore, this work goes a step further compared to the state of the art by also exploring other revenue sources beyond price arbitrage for LAES. Indeed, the authors aim to economically valorise the exhaust stream of air at the outlet of the expansion phase to be used as compressed/clean dry air (CDA). Noteworthy, industries like semiconductor fabrication facilities (fabs) use CDA to drive pneumatic components of manufacturing equipment, regulate valve operations, and sanitize materials and machinery [34]. Production of the CDA requires high-energy penalty filtering and dehumidifying processes (dew point of -20 °C or even below), making it one of the highest energy demands in a semiconductor fab, accounting for around 20% of the total electricity consumption [34]. For humid climates such as Singapore, the electricity consumption might be even higher than the one reported in literature. Since air purification is necessary for the air liquefaction process and the moisture and CO<sub>2</sub> level is considerably low

[9,35], the dryness and cleanliness of the LAES outlet air, on the other hand, is qualified enough to serve as the CDA for wafer fabs.

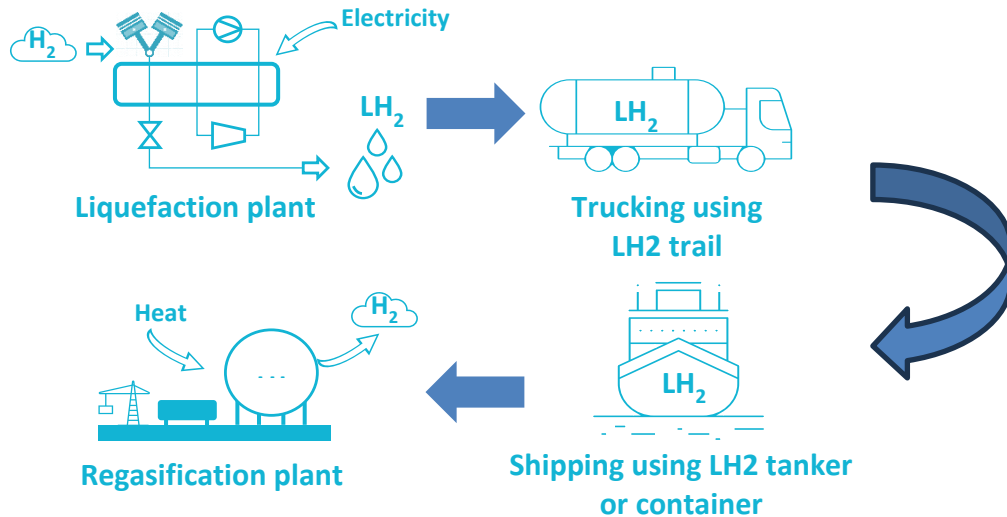


Fig. 2. Liquid hydrogen supply chain concept.

Therefore, this study proposes an integrated LAES energy system for  $LH_2$  regasification, expanding upon existing research primarily focused on LNG integration. While a recent work in literature introduces the concept of waste cold recovery from  $LH_2$  regasification [27], this study advances the field by: 1) investigating the techno-economic feasibility of integration at a commercial LAES scale; 2) proposing a novel configuration incorporating a cryogenic Rankine cycle for optimal waste cold utilization during peak demand periods when LAES discharges; 3) introducing the economic valorization of clean dry air (CDA) discharged by LAES as an additional revenue stream; and 4) conducting a sensitivity analysis on varying electricity tariffs to assess their impact on the economic performance of the integrated system. While energy arbitrage is the most common function of LAES, this study demonstrates its multi-energy and multi-streams capability, allowing operators to access revenues from  $LH_2$  regasification service fees and CDA sales, thus enhancing its economic viability.

The paper presents the following sections. Section 2 concerns the description of the proposed LAES configurations whereas the methodology and the techno-economic assumptions used to develop the numerical models are presented in Section 3. In Section 4, the assessment of the techno-economic results is performed for the different configuration analyzed; Section 5 presents the main conclusions.

## 2. System description

The configuration of the stand-alone LAES system taken as reference is presented in Fig. 3 which clearly highlights the different phases of the energy storage system's operation. A 50  $MW_e/150 MWh_e$  grid-scale LAES plant, with a power to energy ratio close to that proposed in [36], was taken as reference for the LAES scale. In the figure, arrows of different colours represent various flow streams: black solid lines indicate air flow, red solid lines denote thermal oil circulation for HGWS, and blue lines depict nitrogen flow for HGCS, with solid lines for the charging phase and dashed lines for the discharge phase.

The system comprises five main processes: i) charge phase - air liquefaction plant, ii) liquid air storage phase, iii) hot thermal energy storage (high grade warm storage-HGWS), iv) cold thermal energy storage (high grade cold storage-HGCS) and v) a discharge phase – direct expansion process.

Aiming to efficiently liquefy the ambient air, the charge phase employs the Kapitza thermodynamic cycle [37]. It consists of three air-intercooled compression stages driven by the off-peak electricity, followed by the cold box, a multi-stream heat exchanger that enables the working fluid to achieve cryogenic temperatures. After the high-pressure air enters the cold box for cooling, a fraction of the processed air flow expands, produces work in the turbine CT (generating electricity in the generator set G), and cools down. In this way, the expansion process leads to a large temperature reduction of the air stream. The other fraction is throttled through a Joule-Thomson valve to the required storage pressure: the liquid air is therefore extracted from the phase separator and stored in pressurized tanks. The not-liquefied air (point 13A) is used to cool down the high pressure stream in the recuperative process in the cold box. The efficiency of the compression process is directly proportional to the amount of waste heat generated during this phase: this exergetically valuable stream is recovered through a heat transfer fluid in a dedicated double-tanks thermal energy storage (HGWS). The discharge phase, activated during the peak electricity hours, enables the electricity to be fed back into the grid. It involves a liquid air pump section (cryoP1), an evaporator and a multi-stage reheated expansion train that utilizes the waste heat stored in the HGWS. To enhance the round-trip efficiency, the waste cold released during the liquid air evaporation is captured in a packed bed cold thermal energy storage system (HGCS). This stored cold is later used to cool the incoming air in the cold box in the next cycle, improving the overall system performance. Nitrogen and thermanol 66 are used as heat transfer fluids for the HGCS and HGWS loops, respectively. More exhaustive descriptions of the stand-alone system can be found in other authors' work (Refs[18,38,39]).

The integrated system LAES-LH2-CRC (**Fig. 4**) perfectly resembles the stand-alone system regarding the core of the energy storage system, however with a significant difference. In the figure, green dashed lines indicate hydrogen flow and black dashed lines denote nitrogen as working fluid for the CRC. The liquid hydrogen is first pumped at the pressure (30 bar) required by the power plant and subsequently evaporated releasing a high exergetically valuable cold streams. Depending on the LAES operation phase, this stream will be diverted through a three-way valve in the different sections of the energy storage plant, as shown in the integration box on the right side of **Fig. 4**.

During the charge phase (air liquefaction & waste cold utilization/LH<sub>2</sub> regasification), after the ambient air is purified and dried, it enters the cascade compressor unit C1-C3 to increase its pressure. The waste heat produced during the compression process is stored by means of a dedicated hot thermal energy storage (HGWS) using diathermic oil as heat transfer fluid (HTF) and storage medium. During this period, the waste cold released from the regasification of liquid hydrogen (LH<sub>2</sub>), which occurs at an extremely low temperature of ~ -250°C (point 2H in **Fig. 4**), is harnessed to pre-cool and assist the liquefaction of ambient air within the cold box. This process significantly reduces the energy demand of the air liquefaction cycle by lowering the temperature of the incoming compressed air before it reaches cryogenic conditions. The integration takes place through a series of heat exchangers inside the cold box, where the ultra-cold LH<sub>2</sub> gas stream absorbs heat from the high-pressure ambient air, effectively bringing it closer to its liquefaction point. After being processed by the phase separator, the produced liquid air enters the liquid air storage tank LA for storage, and the gaseous air returns to the cold box again. During the discharge phase (Liquid air expansion & waste cold utilization/LH<sub>2</sub> regasification), the liquid air is pressurized by the liquid air pump, evaporates in the evaporator, and expands in several stages of turbines to generate electricity back to the grid. During this period, the waste cold from liquid air regasification is stored in the cold thermal energy storage (HGCS) and is supplied to the cold box to support air liquefaction. The waste cold released by the LH<sub>2</sub> regasification is utilized to further

enhance the electricity generation by means of a cryogenic Rankine cycle (CRC). The remaining waste heat available at the outlet of the superheating process represents the heat source of the CRC. Due to its cryogenic operational temperatures perfectly matching the regasification temperature of LH<sub>2</sub>, its fire extinguisher and its hazardous free capabilities, nitrogen was chosen as the main working fluid for the CRC. The CDA at the turbine outlet is directly provided to a wafer fab for its manufacturing processes.

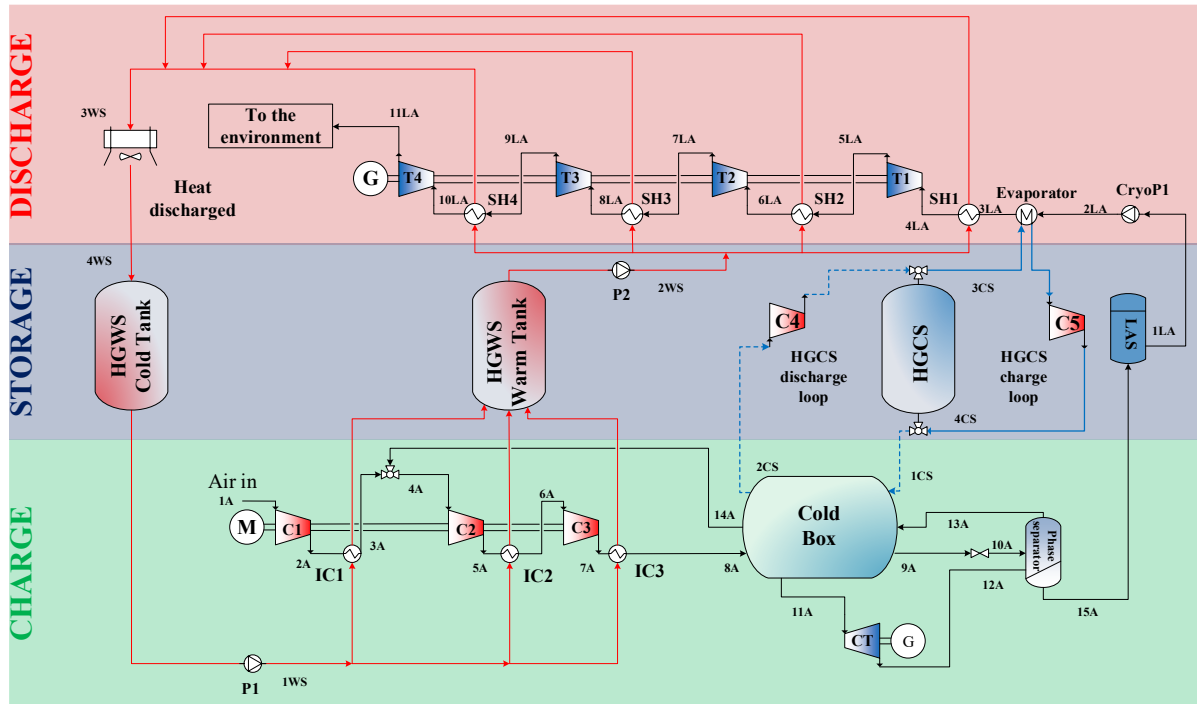


Fig. 3. Stand-alone LAES process flow diagram process.

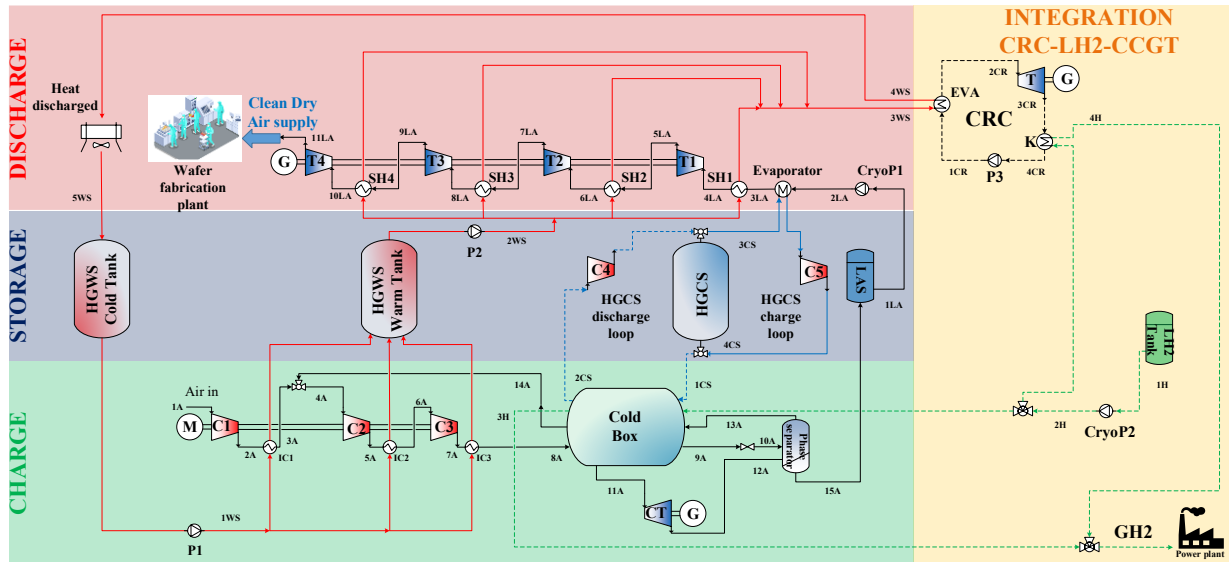


Fig. 4. Integrated LAES-LH<sub>2</sub>-CRC process flow diagram process.

### 3. Mathematical models

The technical analysis was carried out by developing and implementing MATLAB R2023b routines to model the different sections and components of the LAES stand-alone and integrated system. Notably, all the implemented models were developed in the authors' previous works. The

dynamic thermodynamics model developed by Tafone et al. [18] is used to simulate the performance of the LAES exploiting the waste cold supplied by the LH<sub>2</sub> regasification process. The steady-state Rankine cycle model developed by Pili et al. [40], and implemented in Tafone et al. [41], is used to simulate the cryogenic Rankine cycle exploiting the waste cold potential from the LH<sub>2</sub> regasification process. As already introduced in Section 0, for the regasification plant, LH<sub>2</sub> is supplied to guarantee a 30% blend of hydrogen into natural gas to the 600 MW advanced combined cycle gas-turbine (CCGT) power plant developed by Keppel Infrastructure in Singapore [42]. For the wafer fab, CDA is supplied to save the operational cost of the air purifiers and air dehumidifiers. The fluids thermo-physical properties were retrieved using Coolprop as open-source thermodynamic property library [43]. In this study, the CoolProp library was selected due to its widespread use and established reliability in cryogenic applications. CoolProp provides thermodynamic properties based on high-fidelity equations of state, including the Helmholtz free energy formulation, which has been validated against experimental data for cryogenic fluids such as nitrogen and hydrogen [44]. In order to further demonstrate the accuracy of Coolprop, Refprop data (one of the most accurate library package for cryogenics, as shown in Son et al. [45]) has been retrieved from NIST website [46] and compared with the one obtained from Coolprop for the regasification of liquid hydrogen at the same pressure (30 bar). As shown in **Table 1**, the results are quite in good agreement.

**Table 1.** Coolprop validation against Refprop thermo-physical data.

Parameters	Coolprop	Refprop	Unit	$\Delta\%$
$T_{2H}$	-250	-250	°C	
$p_{2H}$	30	30	bar	
$h_{2H}$	50372	50326	J/kg	
$T_{3H}$	15	15	°C	
$p_{3H}$	30	30	bar	
$h_{3H}$	3797004	3797000	J/kg	
$\Delta h_{regasification}$	3746632	3746674	J/kg	0.001%

Furthermore, the following assumptions were made for the thermodynamic analysis:

- The analysis applies a general framework that considers energy and mass conservation within control volumes encompassing the primary components of LAES, CRC, and CCGT systems.
- The model does not account for pressure losses across the heat exchangers.
- Dry air is assumed to be the working fluid and storage medium for the LAES system [47].
- Nitrogen is considered the working fluid in the cryogenic Rankine cycle [47].
- It is assumed that the storage tanks, heat exchangers, and separators are thermally insulated.
- Therminol 66 and nitrogen are used as heat transfer fluids for HGWS and HGCS, respectively.

### 3.1. Turbomachinery devices and cryogenic pump

The performance of turbomachinery devices was modeled using the polytropic efficiency ( $\eta_p$ ) to calculate the compression and expansion work of each  $i$ -th stage:

$$\dot{W}_{Compr,i} = \frac{\dot{m}_{wf,Compr,i}(h_{in,Compr,i} - h_{out,poly,Compr,i})}{\eta_{poly,Compr,i}} \quad (1)$$

$$\dot{W}_{T,i} = \eta_{poly,T,i} \dot{m}_{wf,T,i}(h_{in,T,i} - h_{out,poly,T,i}) \quad (2)$$

$$\dot{W}_{CT,i} = \eta_{poly,CT,i} \dot{m}_{wf,CT,i} (h_{in,CT,i} - h_{out,poly,CT,i}) \quad (3)$$

The polytropic efficiency establishes a thermodynamic correlation between the temperature and pressure ratios based on the ratio of the isobaric specific heat capacity to the isocoric specific heat capacity ( $\gamma$ ):

$$\frac{T_{Compr,out}}{T_{Compr,in}} = \left( \frac{p_{Compr,out}}{p_{Compr,in}} \right)^{\frac{\gamma-1}{\gamma} \frac{1}{\eta_{p,Compr}}} \quad (4)$$

$$\frac{T_{T,out}}{T_{T,in}} = \left( \frac{p_{T,out}}{p_{T,in}} \right)^{\frac{\gamma-1}{\gamma} \eta_{p,T}} \quad (5)$$

The correlations developed by Wilson [48] are used to compute the polytropic efficiencies based on the pressure ratios:

$$\eta_{poly,Compr} = 0.91 - \frac{\left( \frac{p_{Compr,out}}{p_{Compr,in}} \right) - 1}{300} ; \quad (6)$$

$$\eta_{poly,T} = 0.90 - \frac{\left( \frac{p_{T,in}}{p_{T,out}} \right) - 1}{250} . \quad (7)$$

A comparable method utilizing a fixed isentropic efficiency [38] is applied to the cryogenic pump during the discharge phase, ensuring the working fluid is pressurized from the storage level to the discharge pressure:

$$\dot{W}_{Pump,i} = \frac{\dot{m}_{wf,Pump} (h_{in,Pump} - h_{out,iso,Pump})}{\eta_{iso,Pump}} \quad (8)$$

### 3.2. Two streams and multi-streams heat exchangers

A traditional  $\varepsilon$ -NTU approach combined with energy balance equation has been applied to the two-stream heat exchangers in LAES systems, including the intercoolers, evaporator, and superheaters. By assuming a counterflow configuration, the effectiveness of each heat exchanger is calculated as:

$$\varepsilon = \frac{1 - \exp[-NTU(1 - C^*)]}{1 - C^* \exp[-NTU(1 - C^*)]} \quad (9)$$

where  $C^*$  is the thermal capacity ratio of the two streams ( $\dot{C}_{min}/\dot{C}_{max}$ ).

The cold box, a crucial component in the liquefaction process, consists of two heat exchangers arranged in series, handling four distinct streams: the compressed air to be liquefied, the recycled air in a saturated vapor state from the phase separator, the nitrogen stream recycled from the HGCS and the liquid hydrogen to be regasified. Given the significant variation in the working fluid's specific heat ( $c_p$ ) with temperature, the pinch point approach was adopted to address the potential formation of a minimum temperature difference (pinch point) within the system. The heat exchanger was numerically discretized into several sub-heat exchangers along the flow path, with boundary conditions for each segment aligned with adjacent sections. The discretization method applied is the cell-by-cell approach [49], which involves a one-dimensional discretization of the heat exchanger. The energy conservation equation is applied to each control volume individually,

as illustrated in **Fig. 5**. The number of control volumes selected for each heat exchanger is 50 and it has been selected to guarantee a good compromise between the accuracy of the results and the computational cost.

Energy balances were conducted for each sub-heat exchanger to determine the inlet and outlet temperatures on both the hot and cold sides (**Fig. 5**):

$$\dot{Q}_{H,i} = \dot{m}_{wf,H}(h_{H,i} - h_{H,i+1}) \quad (10)$$

$$\dot{Q}_{C,i} = \dot{m}_{wf,C}(h_{C,i} - h_{C,i+1}) + \dot{Q}_{HGCS,i} + \dot{Q}_{LH_2,i} \quad (11)$$

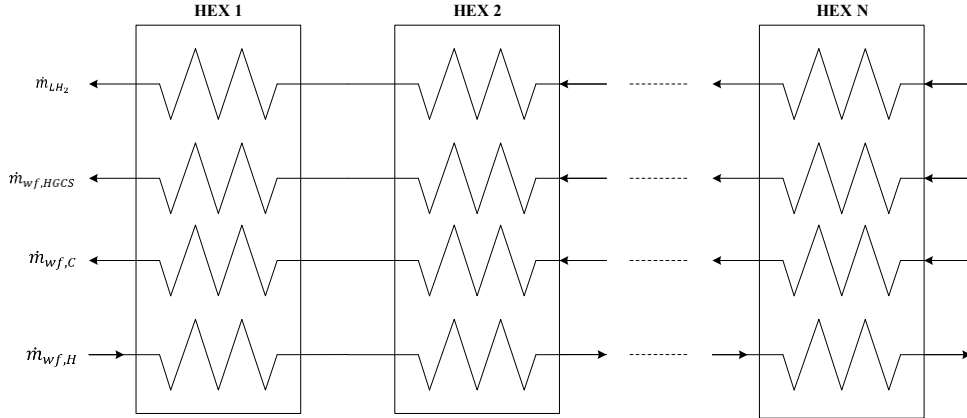


**Fig. 5.** Multi-streams heat exchanger discretization approach. Adapted from Ref.[18].

### 3.3. Packed-bed thermal energy storage

The packed bed thermal energy storage (TES) system plays a vital role in the LAES system and is commonly employed in the chemical and petrochemical industries, often functioning as catalytic reactors. Its packed bed configuration enhances heat transfer efficiency between the heat transfer fluid (HTF) and the storage medium by maximizing the heat transfer surface-to-volume ratio. This is accomplished by filling the storage volume with materials such as spheres, irregularly shaped pebbles, encapsulated phase change materials (PCMs), or other structured geometries, through which the HTF flows. As illustrated in the schematic of the HGCS loop in **Fig. 6**, the HGCS charge phase corresponds to the LAES discharge phase (i.e., liquid air regasification and subsequent expansion). During this phase, the HTF enters the HGCS from the bottom at an inlet temperature  $T_{HTF,in,ch}$  and exits at the top after transferring cold energy to the storage medium, leaving at  $T_{HTF,out,ch}$ . Conversely, the HGCS discharge phase aligns with the LAES charge phase (i.e., the air liquefaction process). During this phase, the HTF flow direction reverses, entering from the top at  $T_{HTF,in,d}$  and exiting from the bottom at the desired temperature  $T_{HTF,out,d}$  to support the air liquefaction process. The inlet temperatures are the boundary conditions for the partial differential equation in Eq. (13).

To evaluate the thermal performance of the HGCS, the energy conservation equations governing heat transfer within the packed bed must be solved. Two unsteady, one-dimensional energy equations were developed to model the transient temperature profiles of both the heat transfer fluid and the particle phase within the HGCS.

For the heat transfer fluid phase:

$$\varepsilon \rho_{HTF} c_{p,HTF} \left( \frac{\partial T_{HTF}}{\partial t} + u_{HTF} \frac{\partial T_{HTF}}{\partial x} \right) = \varepsilon k_{HTF} \frac{\partial^2 T_{HTF}}{\partial x^2} - h_v (T_{HTF} - T_s) + \frac{U_w \pi D}{A_{bed}} (T_{amb} - T_f) \quad (12)$$

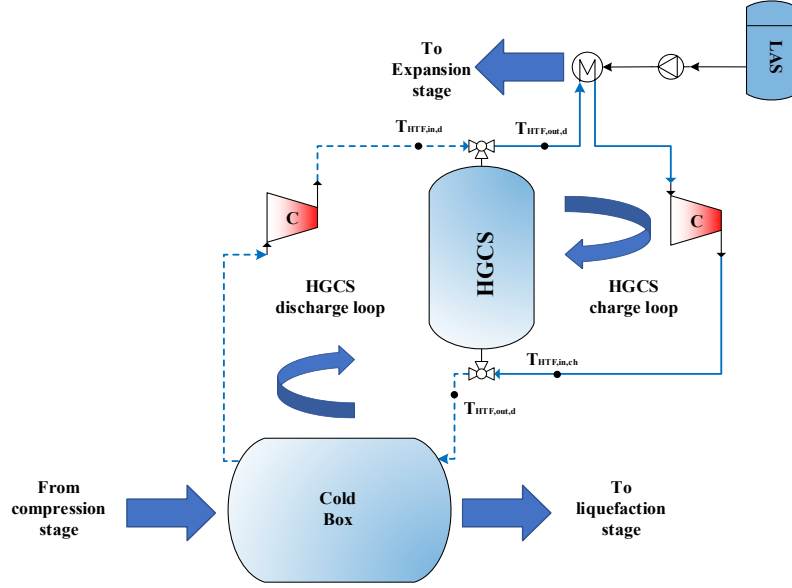


Fig. 6. LAES process schematic with a focus on HGCS operation. Adapted from [17].

For the solid phase:

$$(1 - \varepsilon)\rho_s c_{p,s} \frac{\partial T_s}{\partial t} = (1 - \varepsilon)k_s \frac{\partial^2 T_s}{\partial x^2} + h_v(T_{HTF} - T_s) \quad (13)$$

Additional and more exhaustive information regarding the numerical model can be found in [50] and [18]. **Table 2** reports the physical properties of the storage material employed.

**Table 2.** Storage material properties [17].

Parameters	Value	Unit
Material	Quartzite	-
$\rho$ , Density	2630	$kg/m^3$
$c_p$ , Specific heat	0.71	$kJ/kg K$
$k$ , Thermal conductivity	1.83	$W/m K$
$d_p$ , Particle diameter	0.015	$m$

### 3.4. High grade warm storage

The high-grade warm storage (HGWS) is a sensible heat thermal energy storage modelled as a two tanks liquid storage system filled with diathermic oil (Therminol 66) which represents both as the HTF and storage medium. A steady-state model of each tank is applied during LAES operation since uniform temperatures approximation can be reasonably considered for both tanks [14]:

$$\int_0^{t_{ch}} \dot{m}_{HGWS,in} dt = \int_0^{t_d} \dot{m}_{HGWS,out} dt \quad (14)$$

### 3.5. Cryogenic Rankine cycle

The Cryogenic Rankine cycle system was modeled by using a MATLAB design routine previously developed and validated in [51–53]. Validation tests were carried out both with a Dymola model and an existing ORC system, showing deviations below 2 % and 10 % in net power output, respectively [51,52].

A supercritical CRC system without recuperator is considered here. After a preliminary screening of possible working fluids for cryogenic applications, nitrogen was identified as suitable candidate, given its low environmental impact, high thermal stability, good thermodynamic performance and foremostly its fire extinguisher properties to prevent potential hazards in presence of a flammable fluid such as hydrogen.

The design routine is based on steady-state mass and energy balances on control volumes around the main CRC components:

$$\dot{m}_{wf,in} = \dot{m}_{wf,out} = \dot{m}_{wf} \quad (15)$$

$$\dot{m}_{wf,in}h_{wf,in} + \dot{Q} - \dot{W} = \dot{m}_{wf,out}h_{wf,out} \quad (16)$$

where  $\dot{m}_{wf}$  is the working fluid mass flow rate,  $h_{wf}$  is the specific enthalpy of the working fluid,  $\dot{Q}$  is the heat transfer rate either from the heat source ( $\dot{Q} > 0$ ) or heat sink ( $\dot{Q} < 0$ ) and  $\dot{W}$  the mechanical power transferred from the turbine ( $\dot{W} > 0$ ) or pump ( $\dot{W} < 0$ ).

The heat sink for the CRC unit is represented by the waste cold available at the regasification process of the liquid hydrogen at  $-250.4$  °C and 30 bar. The heat source is the waste heat available from the diathermic oil at the outlet of the superheating process of the LAES (point 3WS in **Fig. 4** at  $T = 68.6$  °C and  $p = 1.5$  bar) during the discharge phase.

Pressure, heat and electric losses in the CRC system are not considered in the mathematical model. The heat exchangers were discretized in control volumes according to the number of phases (liquid, two-phase and vapour). The net power output of the CRC unit is calculated as follows:

$$\dot{W}_{net,CRC} = \dot{W}_T\eta_G + \frac{\dot{W}_{Pump}}{\eta_{Pump,M}\eta_{Pump,I}} = \dot{m}_{wf}(h_{wf,T,in} - h_{wf,T,out})\eta_G - \dot{m}_{wf}\frac{h_{wf,Pump,in} - h_{wf,Pump,out}}{\eta_{Pump,M}\eta_{Pump,I}} \quad (17)$$

where  $\eta_G$ ,  $\eta_{PM}$  and  $\eta_{PI}$  are the efficiencies of the electric generator and pump electric motor, pump frequency converter, which were assigned representative values of 90%, 85%, and 95%, respectively. The empirical correlations developed by Macchi and Astolfi [54] for single-stage turbines were used to estimate the isentropic efficiency of the CRC turbine. The design isentropic efficiency of the pump was fixed to 70 % [55].

The objective function to maximize is the net electrical efficiency  $\eta_{el,net,CRC}$ , defined as follows:

$$\eta_{el,net,CRC} = \frac{\dot{W}_{net,CRC}}{\dot{Q}_{EVA,CRC}} \quad (18)$$

where  $\dot{Q}_{EVA,CRC}$  is the overall thermal power received from LAES at the evaporation section of the CRC unit.

Additional and more exhaustive information regarding the numerical model and the optimization routine can be found in [41].

### 3.6. Techno-economic analysis and optimization

A detailed techno-economic analysis is performed to evaluate the economic benefits of the integrated energy system. The assumptions, merits and terms used in this part are listed in **Table 3**. It is worth to highlight that the boundary of the economic analysis is defined around the LAES

and CRC plants, and thus it excludes the liquid hydrogen pumping cost and the external regasification unit dedicated to the power plant when LAES and CRC are not operating. This approach ensures a consistent comparison by isolating the economic performance of the integrated system without attributing additional costs that would be incurred regardless of LAES integration. Including these costs would misrepresent the specific impact of the proposed system on the overall economics.

The total investment cost of LAES has been computed by applying the module costing technique [56] to calculate the bare module cost ( $C_{BM}$ ) of each LAES component, modified by the chemical engineering plant cost index ( $CEPCI$ ) to reflect inflation effects of current time from any past year  $X$ :

$$CAPEX_{LAES} = \sum C_{BM,i} \left( \frac{CEPCI_{2022}}{CEPCI_X} \right) \quad (19)$$

Since such bare module component cost correlations are associated with significant uncertainties and the underlying data is usually not available and regionally specific, correlations from multiple sources are used for each component. In this paper, four methods are used to calculate and compare the bare module cost of each component, obtained from Turton et al. [56], Seider et al.[57], Couper et al.[58], Peters et al. [59] and Hewitt and Pugh [60]. The main idea is to assess the costs of each component through the application of the four main correlation methods, generating mean estimates that are subsequently summed up to derive system cost estimates. For the sake of comprehensiveness, a brief description of the assumptions for the cost correlations implemented for the main components (absorption/stripper columns, heat exchangers, compressors and vessels) is reported in **Table 4**.

**Table 3.** Assumptions for the techno-economic analysis

Parameters	Value	Unit	Reference
<i>Lifetime</i>	35	year	[61]
$ET_{off,peak}$	0.1394	USD/kWh <sub>e</sub>	[62]
$ET_{peak}$	0.2154	USD/kWh <sub>e</sub>	[62]
$n_{cycle}$	365	Cycle/year	Assumption
$OPEX_{LAES,Power}$	12.03	USD/kW <sub>e</sub> /year	[63]
$OPEX_{LAES,Energy}$	0.00289	USD/kWh <sub>e</sub> /year	[63]
$OPEX_{CRC}$ (%CAPEX)	2.5	%	[64]
<i>Clean dry air specific consumption (<math>SC_{CDA}</math>)</i>	0.147	kWh <sub>e</sub> /m <sup>3</sup>	[65]
<i>CDA Utilization factor (<math>\mu</math>)</i>	0.70	-	[65]
$CEPCI_{2022}$	816	-	[66]
$i$	5	%	Assumption

To estimate the capital cost of the cryogenic Rankine cycle, the following correlation, developed by Xiao et al. [67] and obtained from a market survey data during the past 10 years, has been implemented to retrieve the specific investment cost (SIC) expressed in USD/kW<sub>e</sub> as a function of the net power output of the CRC unit as expressed in Eq.(16):

$$SIC_{CRC} = - 678 \ln(\dot{W}_{net,CRC}) + 6725.4 \quad (20)$$

**Table 4.** Cost correlations overview for the LAES capital cost evaluation.

Components	Cost correlations	Notes
<b>Turbines and compressors</b>	Turton et al. [56] Seider et al. [57] Couper et al. [58] Peters et al. [59]	Correlations based on the nominal power. Carbon-steel construction.
<b>HGCS</b>	Turton et al. [56] Seider et al. [57] Couper et al. [58] Peters et al. [59]	Correlations based on volume and maximum pressure. Costed as pressure vessel filled with storage material. Carbon-steel construction.
<b>Liquid Storages &amp; Pumps</b>	Turton et al. [56] Seider et al. [57] Couper et al. [58] Peters et al. [59]	Correlations based on the storage tank volume. Costed as liquid storage tanks with pumps.
<b>Two-streams HEX</b>	Turton et al. [56] Seider et al. [57] Couper et al. [58] Peters et al. [59]	Correlations based on the heat transfer area and maximum pressure. Floating head and carbon-steel construction.
<b>Multi-streams HEX</b>	Hewitt & Pugh [60]	Correlation based on the estimation of the core volume. Costed as brazed aluminium plate-fin heat exchanger.

The first law analysis was implemented to compute the premier performance index of the LAES charge phase, namely the **liquefaction specific consumption**, computed as:

$$SC_{LAES} = \frac{\int_0^{t_{ch,LAES}} \dot{W}_{net,ch} dt}{\int_0^{t_{ch,LAES}} \dot{m}_{LA} dt} \quad (21)$$

where  $\dot{W}_{net,ch}$  and  $\dot{m}_{LA}$  are the instantaneous net power consumption and liquid air production during the LAES charge phase, respectively.

The premier key performance indicator of the LAES energy storage system is represented by the round-trip efficiency, computed as follows:

$$\eta_{RT} = \frac{\int_0^{t_d} \dot{W}_{net,d} dt + \int_0^{t_d} \dot{W}_{net,CRC} dt}{\int_0^{t_{ch}} \dot{W}_{net,ch} dt} \quad (22)$$

where  $\dot{W}_{net,d}$  and  $\dot{W}_{net,CRC}$  are the instantaneous net power production during the LAES discharge phase and the CRC operation, respectively.

In order to maximize the round-trip efficiency of the configurations, a design optimization routine similar to the one adopted in Tafone et al. [18] is used. The derivative-free optimization function ‘patternsearch’ from the MATLAB Optimization Toolbox was used, with a step and function tolerance of 1e-6 and a constraint tolerance (necessary to find the required net power output) fixed to 1e-4. **Table 5** summarized the LAES decision variables and reports the upper and lower bounds set in the design optimization routine. The input parameters, constraints and objective function are summarized in **Table 6**.

**Table 5.** Decision variables for LAES design routine.

Decision variables	Lower bound	Upper bound	Unit
$p_{ch}$ Charging pressure	60	160	bar
$p_d$ Discharging pressure	60	160	bar
$p_{sto}$ Storage pressure	1	12	bar
$\Delta T_{pp,SH}$ Pinch-point temperature difference at SH	5	30	K
$x_{CT} = \dot{m}_{11A}/\dot{m}_{8A}$ , Recirculation fraction	0	1	-
$\dot{m}_{LA}$ Mass flow rate of liquid air	80	100	kg/s

**Table 6.** Input parameters, constraints and objective function for LAES optimization routine.

Parameters	Value	Unit
$T_{amb}$ Ambient air temperature	25	°C
Working fluid	Air	-
$\dot{m}_{LH2}$ Liquid hydrogen mass flow	0.74	kg/s
$t_{ch}$ Charging period	6	h
$t_d$ Discharging period	3	h
$\eta_{iso,P}$ Liquid air pump isentropic efficiency	80	%
$\Delta T_{Evaporator}$ Evaporator cold end temperature approach	5	°C
$\eta_{iso,CRC,P}$ CRC pump isentropic efficiency	70	%
$\Delta T_{EVA,CRC,PP}$ CRC Evaporator pinch point temperature difference	5	°C
$\Delta T_{COND,CRC,PP}$ CRC Condenser pinch point temperature difference	5	°C
$p_{HTF,in,ch}$ Charge HTF inlet pressure	1.5	bar
<b>Constraints</b>		
No temperature crossings among working fluid and heat sources / sink		
Pinch point temperature difference at the cold box equal to 2 K		
Discharge power output equal to 50 MW <sub>e</sub>		
<b>Objective function</b>		
Maximum round-trip efficiency (Eq. 21)		

The levelized cost of storage (*LCOS*) describes the ratio of total lifetime cost of the investment in an electricity storage technology divided by its cumulative delivered electricity estimated at each  $n$  step (years) over the total storage lifetime  $N$  (years) discounted with the interest rate  $i$  (%):

$$LCOS = \frac{CAPEX + \sum_n^N \frac{EC}{(1+i)^n} + \sum_n^N \frac{OPEX_{O\&M}}{(1+i)^n} - \sum_n^N \frac{Rev_{CDA}}{(1+i)^n} - \sum_n^N \frac{Rev_{LH2REG,fee}}{(1+i)^n}}{\sum_n^N \frac{E_d}{(1+i)^n}} \quad (23)$$

where *CAPEX* [MUSD] is the capital cost of the system, computed according to the methodology above mentioned; *EC* [MUSD] is the electricity cost required to charge the LAES, calculated as a function of the electricity tariff and the round-trip efficiency [64]; *OPEX<sub>O&M</sub>* [MUSD] represents the operation and maintenance costs of both LAES and CRC; *Rev<sub>CDA</sub>* [MUSD] is the revenue derived from clean dry air sale; *Rev<sub>LH2Reg,fee</sub>* [MUSD] is the revenue associated with LH<sub>2</sub> regasification service; *E<sub>d</sub>* [kWh<sub>e</sub>] is the electricity produced during the discharge phase.

Finally, the discounted pay-back period (*DPBP*) is established by evaluating the number of years (*DPBP*) to achieve a NPV value of zero:

$$DPBP = \{N \mid NPV = 0\} \quad (24)$$

## 4. Results and discussion

The objective of this section is to comparatively assess the performance of the stand-alone LAES and the LAES-LH<sub>2</sub>-CRC configurations to evaluate their technical and economic performance and comprehend under which condition the usage of waste cold from liquid hydrogen regasification might be advantageous. A system-level analysis of a 50 MW<sub>e</sub>/150 MWh LAES plant was conducted. The thermodynamic cycle state points for both the stand-alone and integrated configurations are reported in the Supplementary Data.

### 4.1. Energetic performance analysis

In order to comparatively assess the systems, the following operational conditions were ensured:

- The operating conditions are the same for all the LAES configurations and are based on the techno-economic data provided in Section 3.
- The techno-economic performance data of integrated and stand-alone systems configurations have been reported for steady state temperature profiles established in the HGCS, after 5 charging and discharging cycles.

**Table 7** lists the technological parameters of the integrated and standalone LAES systems. Since the capacities of the two systems are selected to be the same, the discharging power is kept identical whereas the performance of the two systems would differ.

**Table 7.** Technological parameters of the integrated and standalone LAES systems.

Parameters	Standalone LAES	Integrated LAES	Unit
LAES Discharge Power	50.00	50.00	MW <sub>e</sub>
CRC Net Power	-	0.783	MW <sub>e</sub>
$\eta_{RT}$	58.6	67.6	%
Liquefaction Specific consumption	0.252	0.223	kWh <sub>e</sub> /kg <sub>LA</sub>
Specific production	0.148	0.151	kWh <sub>e</sub> /kg <sub>LA</sub>
Heat transfer fluid for LAES HTES	Therminol 66	Therminol 66	-
Working fluid for CRC	-	Nitrogen	-

The results show a global energy efficiency improvement of LAES plant. Indeed, the waste cold recovery from liquid hydrogen regasification boosts the performance of the liquid air production decreasing the specific consumption of the air liquefier by 12 % (from 0.25 to 0.22 kWh<sub>e</sub>/kg<sub>LA</sub>). In turn the round-trip efficiency increases by 15 % due to the combined effect of the performance enhancement of the liquid air production and the additional electricity production from the CRC ( $\approx 800$  kW<sub>e</sub>).

Derived from the first principle approach, the energy balance applied to both charge and discharge phases is graphically represented by the Sankey diagrams in **Fig. 7-Fig. 9**. In these plots, the different energy flows along with their magnitudes are reported and can assist to further capture the differences between the performance behaviours of the two systems. In the charge phase, the advantage of the availability of the waste cold from LH<sub>2</sub> regasification process allows to significantly decrease the power consumption of the air compressors from 44.58 MW to 37.58 MW for the stand-alone and integrated LAES, respectively, reducing in turn the liquefaction specific consumption as shown in **Table 7**. Consequently, due to the enhanced energetic efficiency of the air liquefaction stage, the potentially available waste heat recovery from the intercooling stage is reduced from 45.73 MW to 38.59 MW. Nevertheless, since the amount of waste heat available consistently exceeds the thermal energy requirement for the discharge phase, as already

demonstrated in literature [39,68], this reduction further improves the efficiency of the waste heat recovery system within the integrated LAES, enabling the downsizing of the hot thermal energy storage (HGWS). Focusing on the discharge phase of the integrated LAES system, the utilization of the waste heat is further optimized by the integration of the cryogenic Rankine cycle that utilizes part of the waste heat available at the CRC evaporator (14.89 MW). This, combined with the waste cold from LH<sub>2</sub> regasification acting as heat sink for the CRC, enhances the discharge power of the integrated system, resulting in an additional CRC electric power production of 0.78 MW. Another significant source of heat loss ( $\approx 6$  MW) for both systems is represented by the air discharged at the last turbine stage T4 (Air<sub>out</sub> stream in **Fig. 7b** and **Fig. 9**). Indeed, considering a hypothetical multi-energy LAES, this stream could provide the thermal energy required by a potential district heating community, offering thus an additional storage service that will turn in an additional revenue stream.

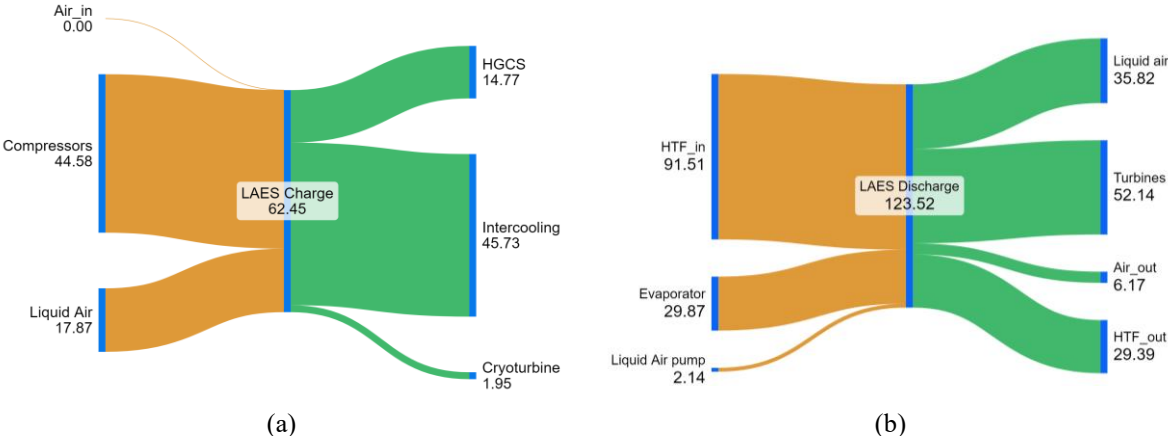


**Fig. 7.** Sankey diagram – Stand-alone LAES charge (a) and discharge (b) phases. All the quantities are in MW.

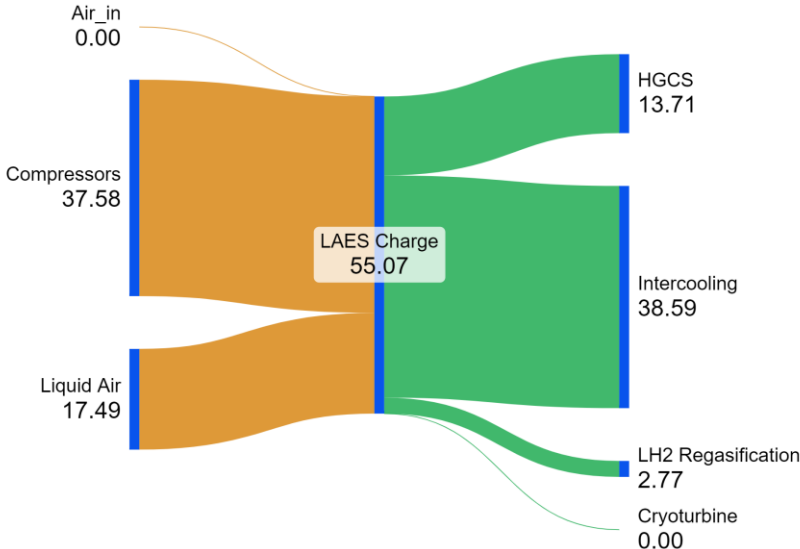


**Fig. 8.** Sankey diagram - Integrated LAES charge phase. All the quantities are in MW.

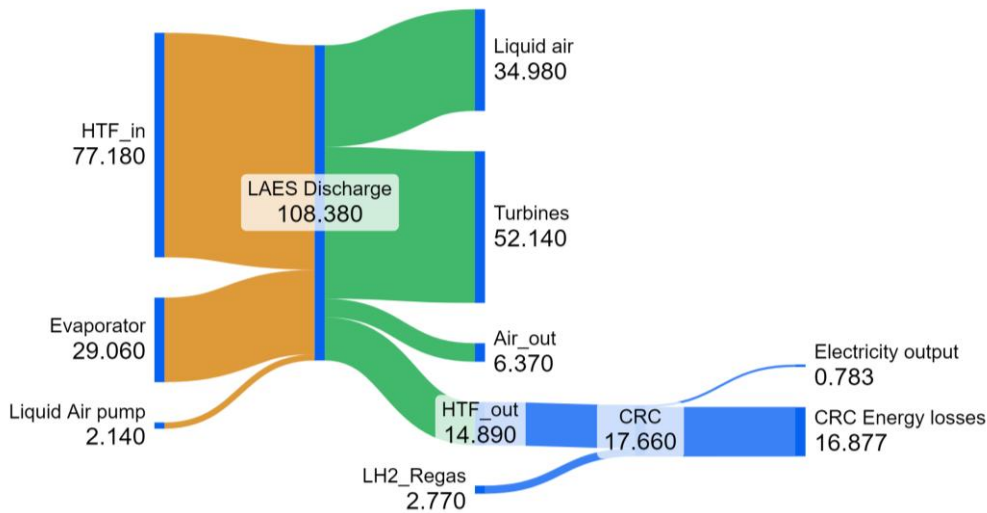


**Fig. 9.** Sankey diagram - Integrated LAES discharge phase. All the numerical quantities are in MW.

#### 4.2. Economic performance analysis

The techno-economic results computed assuming the methodology presented in Section 3.6 are firstly shown in **Fig. 10**, providing the calculated *CAPEX* for both systems. The economic results unexpectedly reveal that the *CAPEX*s of the two systems are almost identical with the integrated system showing a slight lower *CAPEX*. A detailed analysis of the *CAPEX* breakdown offers a clear explanation for this trend. The savings in *CAPEX* from the hot and cold thermal energy storage systems and charging facilities in the integrated system are sufficient to offset the cost of CRC installation, suggesting that the integrated system will slightly reduce overall *CAPEX* despite the high investment cost of the CRC.

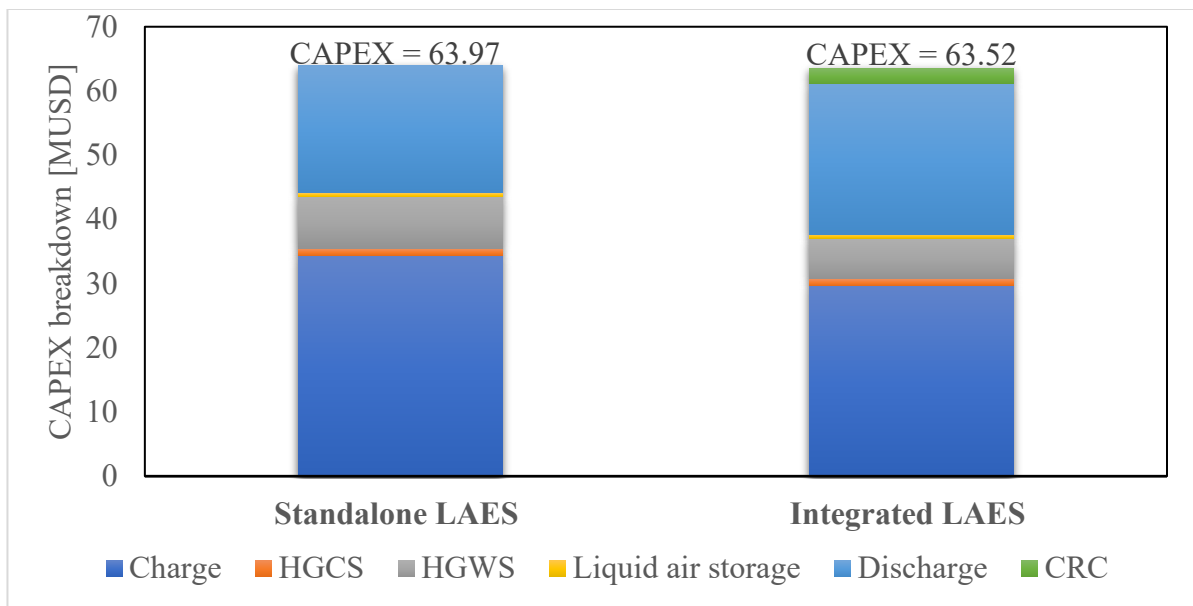


**Fig. 10.** CAPEX comparison of various components in the integrated and standalone LAES systems. The total CAPEXs are reported at the top of each bar.

The cash flows including the operational costs and the revenues associated with the different revenue streams (arbitrage, regasification fee, clean dry air) are reported in **Fig. 11**. The analysis demonstrates how the waste cold from LH<sub>2</sub> regasification affects the economics of the integrated plant in comparison to the stand-alone system.

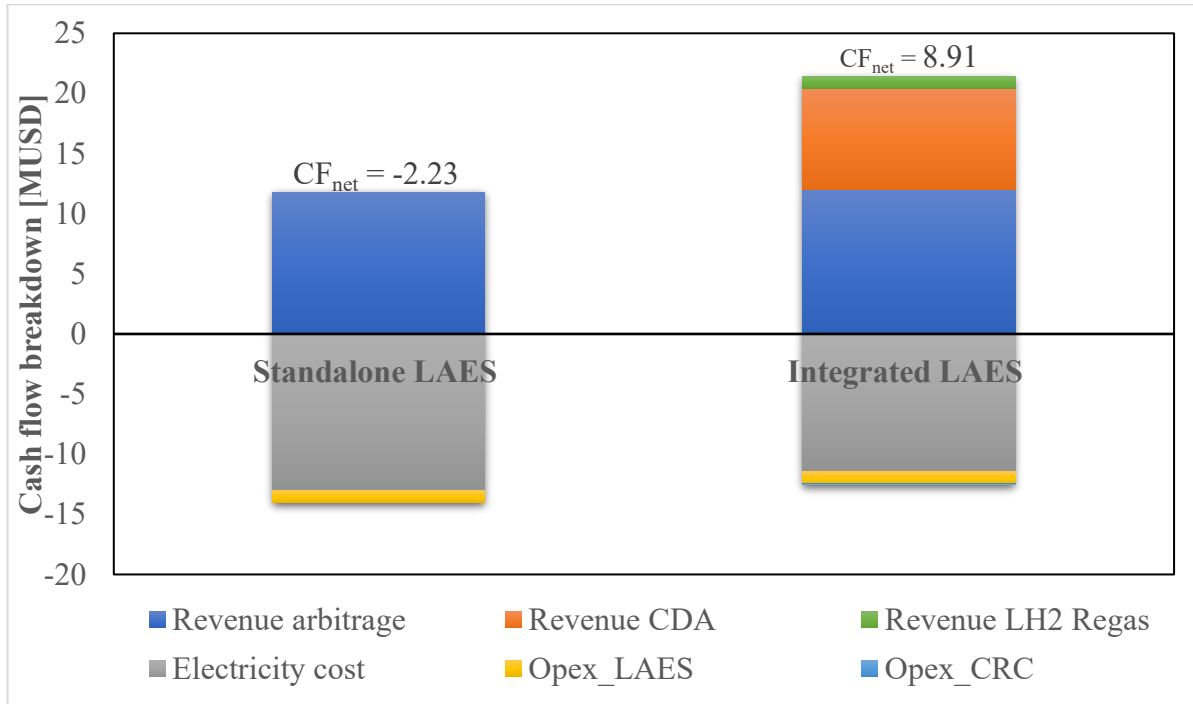


**Fig. 11.** Cash flows comparison of various sources in the standalone and integrated LAES systems. The net CF values are reported at the top of each bar.

Contrary to the *CAPEX* comparison, the revenue (positive cash flows in **Fig. 11**) of the integrated system almost doubles the one of the standalone system, with price arbitrage and CDA generating the largest revenues. Notably, the revenues from CDA sales are approximately of the same magnitude as the arbitrage revenues. On the other hand, the electricity cost expenses are considerably small compared to the standalone system due to the higher round-trip efficiency.

As shown in **Fig. 12**, the high revenue streams of the proposed system lead to a significantly lower *LCOS* which is approximately 60 % lower than that of the standalone system. The pay-back period of the stand-alone LAES is not achieved due to the negative annual cash flow as shown in **Fig. 11**. Again, the revenue due to the price arbitrage does not offset the electricity cost to charge the LAES due to the low round trip efficiency and the low ratio of the peak to off-peak electricity tariff. Specifically, the integrated system achieves an *LCOS* of 0.125 USD/kWh<sub>e</sub> and a *DPBP* of around 9 years. This economic performance favourably compares with other LAES-based and grid-scale energy storage technologies [69].

**Table 8.** Techno-economic comparison of the current work with literature data.

Reference	$\eta_{RT}$ [%]	<i>LCOS</i> [USD/kWh <sub>e</sub> ]	Configuration
Current work	67.6	0.125	LAES integrated with LH <sub>2</sub> regasification
Tafone et al. [64]	52.6	0.385	LAES integrated with organic Rankine cycle
Georgiu et al. [70]	55.0	0.3-0.4	LAES integrated with waste heat
Da Li et al. [71]	110.3	0.090	LAES integrated with solar power plant
Kim et al.[72]	51.0	0.183	LAES integrated with nuclear power plant

As shown in **Table 7**, Tafone et al. [64] analyzed a LAES-ORC integration and reported an LCOS above 0.3 USD/kWh<sub>e</sub>, while Georgiou et al. [70] assessed standalone LAES configurations with LCOS values ranging between 0.3–0.4 USD/kWh<sub>e</sub>. Additionally, Da Li et al. [71] demonstrated that even solar-aided LAES configurations still face LCOS values in between 0.09–0.16 USD/kWh<sub>e</sub>, reinforcing the economic competitiveness of the proposed integration approach. The comparative analysis indicates that the integration with liquid hydrogen regasification brings considerable economic benefits to make LAES a viable option for future grid-scale energy storage.

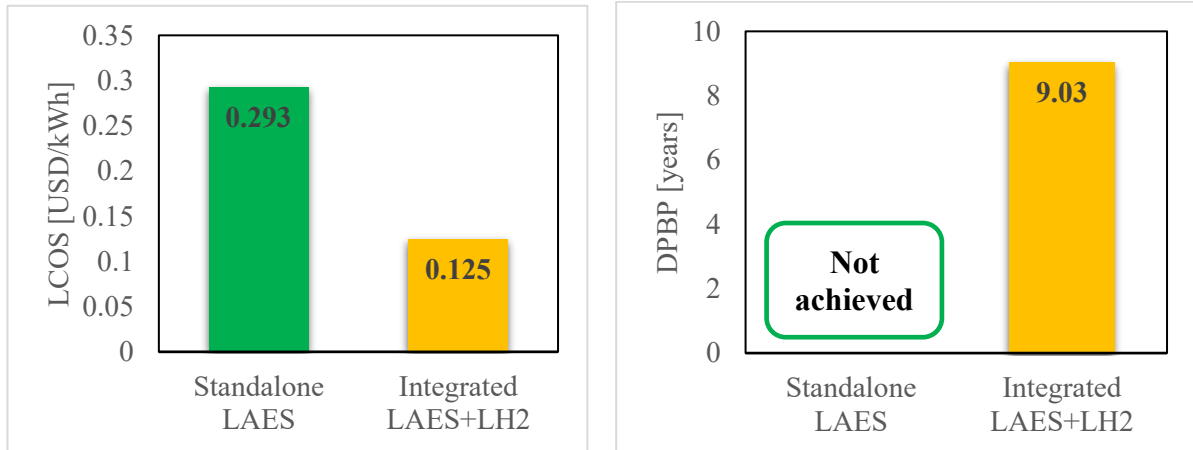


**Fig. 12.** LCOS and DPBP comparison of the standalone and integrated LAES systems.

#### 4.3. Sensitivity analysis case studies (number of cycles, electricity prices and CDA industrial demand)

The current section evaluates the performance of the stand-alone and integrated LAES configurations by varying the number of cycles per year, the electricity tariffs at which LAES is charging and dispatching electricity and the industrial demand of the clean dry air, whose revenue, as shown in **Fig. 11**, is an important pillar for the economic feasibility of the LAES integrated configuration.

**Fig. 13** reports the results of the sensitivity analysis carried out in order to assess the influence of the off-peak electricity tariff and the number of cycles per year over the *LCOS*. Here, a cycle represents a complete sequence of charge and discharge of the energy storage system. This quantity is directly proportional to the total energy discharged by the LAES. As expected, the *LCOS* decreases with an increasing number of cycles per year due to the fixed *CAPEX* and *OPEX* being distributed over a greater energy output. In this study, 365 cycles per year corresponds to one half charge cycle (3 hours) and one half discharge cycle (6 hours) per day. Therefore, operating at more than 365 cycles annually implies multiple charging and discharging events within a single day.

Three different electricity tariffs have been considered: the reference scenario ( $ET_{el,off-peak} = 0.14$  USD/kWh<sub>e</sub>), and two other scenarios where the off-peak electricity tariffs are varied by  $\pm 50\%$ . According to an approximately inverse relation, the *LCOS* decreases as the number of cycles per year, and therefore the total amount of energy discharged increases. In fact, by increasing the amount of energy discharged per year, the *LCOS* decreases significantly since the same *CAPEX* and *OPEX* costs are distributed over a larger amount of energy discharged. Furthermore, **Fig. 13** illustrates how the round-trip efficiency strongly affects the *LCOS*, offering additional insights into the relationship between system efficiency and economic performance. Notably, the gap between the two curves representing the stand-alone configuration and the integrated system increases as the electricity tariff and the number of cycles increase, with an *LCOS* decrease as high as 70 % at number of cycles per year higher than 600.

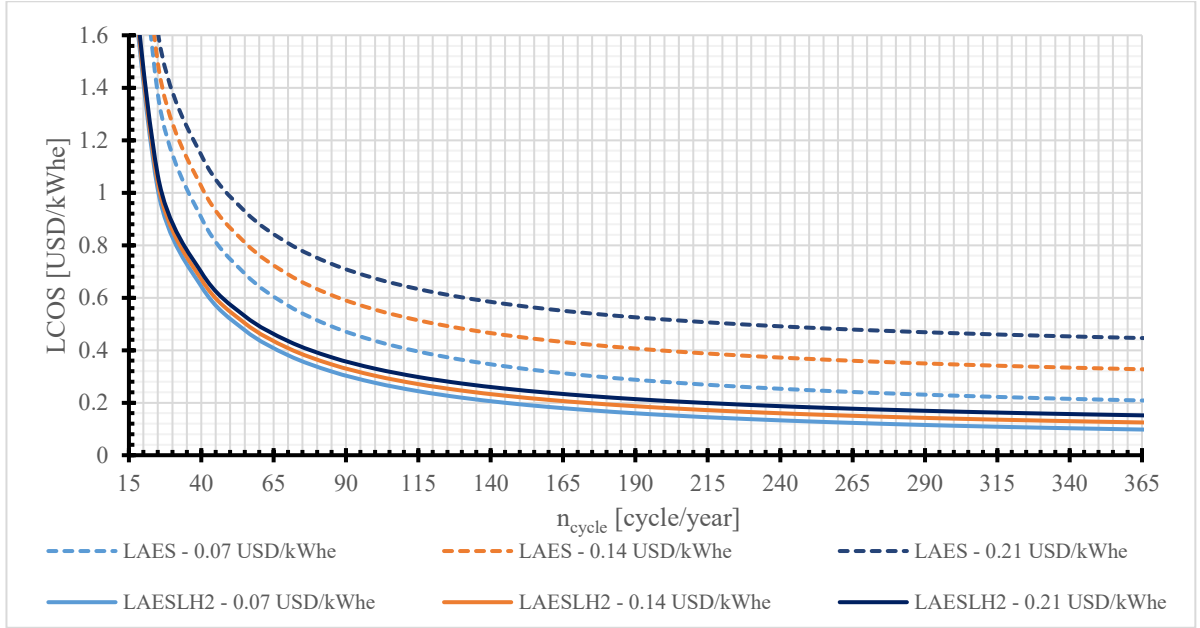


**Fig. 13.** LCOS as a function of the number of cycles per year at different electricity tariffs.

In order to better understand the trends of the KPIs under examination ( $LCOS$  and discounted pay-back period), the results of the sensitivity analysis involving both the electricity tariffs, and the clean dry air demand are plotted in terms of performance heat maps. **Fig. 14-Fig. 16** show the minimum of the  $LCOS$  and the discounted pay-back period at utilization factors of the clean dry air of 10%, 30%, 50% and 70%. Black spots indicate that the pay-back period is either higher than LAES lifetime or not achieved in that specific sensitivity scenario. Electricity tariffs at peak and off-peak period are varied as well between 0.19-0.31 USD/kWh<sub>e</sub> and 0.12-0.18 USD/kWh<sub>e</sub>, respectively. The first thing to note is the significant influence of the clean dry air revenue at every electricity tariff considered. As shown in **Fig. 14** and **Fig. 15** for the integrated LAES system with nominal electricity tariffs ( $ET_{el,offpeak} = 0.1394$  USD /kWh<sub>e</sub> and  $ET_{el,peak} = 0.2154$  USD /kWh<sub>e</sub>), the  $LCOS$  can fall by 50 % achieving a positive discounted pay-back period of 9 years as the utilization factor is varied from 10% to 70%. At low utilization factors of the clean dry air, the  $LCOS$  is highly dependent on the electricity off-peak tariff alone, with a null or weaker influence of the electricity peak tariff, as also demonstrated by **Fig. 16a** considering the stand-alone LAES ( $\mu_{CDA} = 0$ ). Indeed, in these scenarios, the revenues from price arbitrage outweigh the one from clean dry air: as a consequence, the peak electricity tariff has almost no impact on the  $LCOS$ . Conversely, for higher utilization factor of the clean dry air, the  $LCOS$  decline is even stronger since highly depends on both electricity off-peak and peak tariff contributes.

It is worth noting that similar trends are observed for the discounted pay-back period but other factors need to be considered. At lower utilization factors of the clean dry air, the  $DPBP$  is highly sensitive to both off-peak and peak electricity tariffs. As the utilization factor increases, the dependence on the off-peak electricity tariff weakens in comparison to the peak electricity tariff. This shift occurs because the clean dry air revenue becomes increasingly affected by the peak electricity tariff, making it more predominant than the arbitrage revenue component at higher utilization levels. Consequently, the  $DPBP$  decrease significantly.

The final consideration concerns the stand-alone LAES, and it strongly supports findings previously reported in literature. As shown in **Fig. 16b**, only one combination of electricity tariffs ensures an economically feasible pay-back period ( $\approx 20$  years). This outcome perfectly aligns with the conclusions of different studies, which indicate that a stand-alone LAES is not economically viable unless i) waste heat or waste cold are readily available in the vicinity [73–75] and/or a portfolio of different services is provided by the storage operator [76].

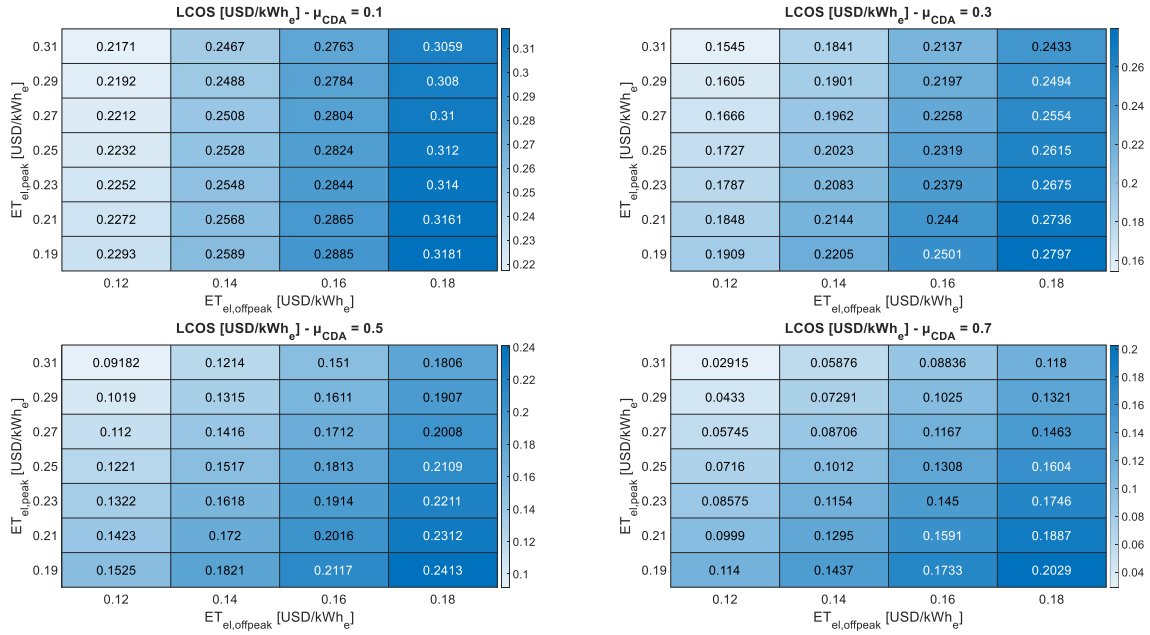


Fig. 14. LCOS performance heat maps. Integrated LAES case study.

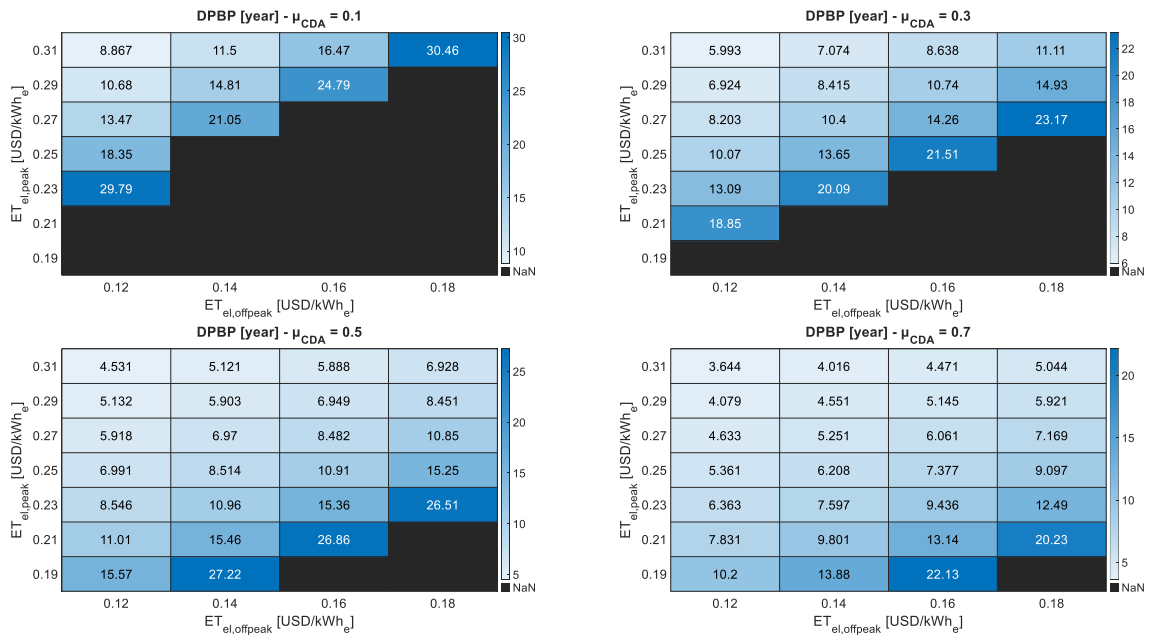


Fig. 15. Discounted pay-back period performance heat maps. Integrated LAES case study.

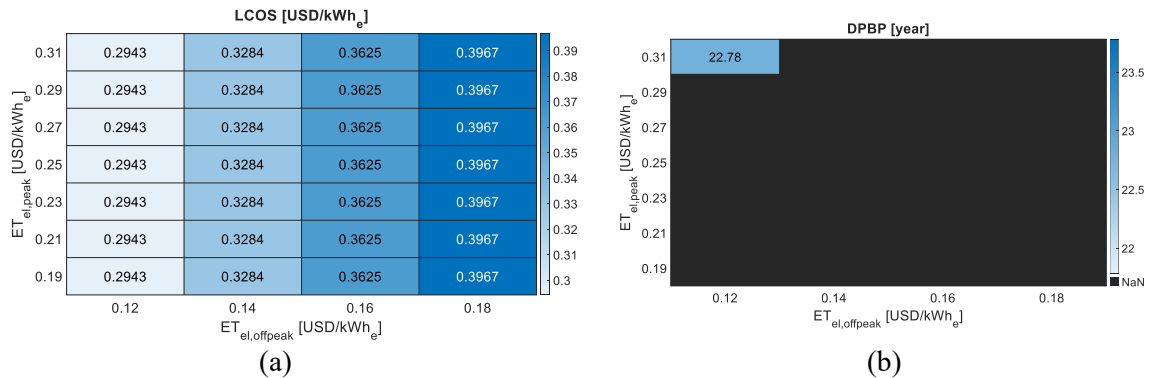


Fig. 16. LCOS (a) and Discounted pay-back period (b) performance heat maps. Stand-alone LAES case study.

## 5. Conclusions

This study proposed and designed a novel integration of Liquid Air Energy Storage with liquid hydrogen regasification and wafer fabrication clean dry air production. The system takes advantage of the otherwise untapped waste cold from LH<sub>2</sub> regasification to enhance the efficiency of the LAES charging process, significantly reducing the energy required for air liquefaction. Additionally, the low-temperature heat transfer fluid and low dew-point outlet air from the LAES discharge are repurposed to support wafer fabrication cooling and CDA production, thereby reducing the energy-intensive cooling costs associated with semiconductor manufacturing.

The integration brings both thermodynamic and economic benefits. By saving the charging and thermal energy storage systems (HGCS and HGWS) costs, the overall capital expenditure is slightly lower than that of a standalone LAES. The combined system generates substantially higher revenue by offering regasification services and electricity arbitrage through CDA supply, resulting in an 80% increase in total revenue compared to a conventional LAES configuration. This enhancement translates into a significant reduction in the levelized cost of storage, which decreases by 60%, from 0.293 USD/kWh<sub>e</sub> to 0.125 USD/kWh<sub>e</sub>. The integration not only improves the economic viability of LAES but also contributes to a more efficient and sustainable approach to energy storage and utilization.

Beyond cost reduction and efficiency improvements, this integration creates a multi-functional energy system that optimally combines energy and material streams. By leveraging synergies between different processes, the system achieves higher overall performance while reducing its discounted payback period, making it a promising candidate for real-world implementation.

Any technical analysis comes with inherent limitations and well-defined boundaries of applicability. Therefore, it is crucial to clearly identify these constraints to guide future research toward meaningful improvements. In this regard, further studies could explore the impact of para-to-ortho hydrogen conversion to enhance the efficiency of waste cold recovery during liquid hydrogen regasification. Additionally, a dynamic analysis of LAES operation could provide deeper insights into how the system responds to fluctuations in liquid hydrogen mass flow and how waste cold recovery might facilitate a quicker LAES startup process. Indeed, while the system's discharge duration is inherently linked to the storage capacity and operational strategy, a comprehensive analysis of dynamic load management and grid interactions would require a dedicated study incorporating real-time electricity market dynamics and demand response mechanisms. Lastly, integrating LAES with a 100% hydrogen-fuelled combined cycle gas turbine (CCGT) at mid-to-micro grid scales (below 10 MW<sub>e</sub>) represents a promising avenue for future research. Such an integration could unlock additional techno-economic benefits, particularly in hydrogen-based power generation and grid stabilization, while offering valuable insights into the feasibility of hybrid energy storage solutions.

## Acknowledgement

This work was financially supported by the Singapore National Research Foundation under its Campus for Research Excellence and Technological Enterprise (CREATE) programme (Grant No.: NRF2022-ITC004-001).

## References

- [1] International Energy Agency (IEA). World Energy Outlook 2022. 2022.
- [2] IPCC. Climate Change 2022 - Mitigation of Climate Change. Cambridge, UK and New York, NY, USA: Cambridge University Press; 2023. <https://doi.org/10.1017/9781009157926>.
- [3] Liang T, Zhang T, Lin X, Alessio T, Legrand M, He X, et al. Liquid air energy storage technology: a comprehensive review of research, development and deployment. *Progress in Energy* 2023;5:012002. <https://doi.org/10.1088/2516-1083/ACA26A>.
- [4] Blakers A, Weber T, Silalahi - D, Laconi N, Licheri F, Stocks M, et al. A review of pumped hydro energy storage. *Progress in Energy* 2021;3:022003. <https://doi.org/10.1088/2516-1083/ABEB5B>.
- [5] Olympios A V, McTigue JD, Farres-Antunez P, Tafone A, Romagnoli A, Li Y, et al. Progress and prospects of thermo-mechanical energy storage—a critical review. *Progress in Energy* 2021;3:022001. <https://doi.org/10.1088/2516-1083/abdbba>.
- [6] Schiebahn S, Grube T, Robinius M, Tietze V, Kumar B, Stolten D. Power to gas: Technological overview, systems analysis and economic assessment for a case study in Germany. *Int J Hydrogen Energy* 2015;40:4285–94. <https://doi.org/10.1016/J.IJHYDENE.2015.01.123>.
- [7] Sharma S, Mortazavi M. Pumped thermal energy storage: A review. *Int J Heat Mass Transf* 2023;213:124286. <https://doi.org/10.1016/J.IJHEATMASSTRANSFER.2023.124286>.
- [8] Budt M, Wolf D, Span R, Yan J. A review on compressed air energy storage: Basic principles, past milestones and recent developments. *Appl Energy* 2016;170:250–68. <https://doi.org/10.1016/j.apenergy.2016.02.108>.
- [9] Liang T, Zhang T, Lin X, Alessio T, Legrand M, He X, et al. Liquid air energy storage technology: a comprehensive review of research, development and deployment. *Progress in Energy* 2023;5:012002. <https://doi.org/10.1088/2516-1083/ACA26A>.
- [10] Borri E, Tafone A, Romagnoli A, Comodi G. A review on liquid air energy storage: History, state of the art and recent developments. *Renewable and Sustainable Energy Reviews* 2021;137:110572. <https://doi.org/10.1016/j.rser.2020.110572>.
- [11] Aliaga DM, Romero CP, Feick R, Brooks WK, Campbell AN. Modelling and simulation of a novel liquid air energy storage system with a liquid piston, NH<sub>3</sub> and CO<sub>2</sub> cycles for enhanced heat and cold utilisation. *Appl Energy* 2024;362:123015. <https://doi.org/10.1016/J.APENERGY.2024.123015>.
- [12] Liang T, Zhang T, Lin X, Tafone A, Legrand M, He X, et al. Liquid air energy storage technology: a comprehensive review of research, development and deployment. *Progress in Energy* 2022. <https://doi.org/10.1088/2516-1083/aca26a>.
- [13] Morgan R, Nelmes S, Gibson E, Brett G. Liquid air energy storage - Analysis and first results from a pilot scale demonstration plant. *Appl Energy* 2015;137:845–53. <https://doi.org/10.1016/j.apenergy.2014.07.109>.
- [14] Sciacovelli A, Vecchi A, Ding Y. Liquid air energy storage (LAES) with packed bed cold thermal storage – From component to system level performance through dynamic modelling. *Appl Energy* 2017;190:84–98. <https://doi.org/10.1016/j.apenergy.2016.12.118>.
- [15] Hüttermann L, Span R. Influence of the Heat Capacity of the Storage Material on the Efficiency of Thermal Regenerators in Liquid Air Energy Storage Systems. *Energy* 2019;174:236–45. <https://doi.org/10.1016/j.energy.2019.02.149>.

- [16] Ryu JY, Alford A, Lewis G, Ding Y, Li Y, Ahmad A, et al. A novel liquid air energy storage system using a combination of sensible and latent heat storage. *Appl Therm Eng* 2022;203:117890. <https://doi.org/10.1016/J.APPLTHERMALENG.2021.117890>.
- [17] Tafone A, Borri E, Cabeza LF, Romagnoli A. Innovative cryogenic Phase Change Material (PCM) based cold thermal energy storage for Liquid Air Energy Storage (LAES) – Numerical dynamic modelling and experimental study of a packed bed unit. *Appl Energy* 2021;301:117417. <https://doi.org/10.1016/J.APENERGY.2021.117417>.
- [18] Tafone A, Romagnoli A. A novel liquid air energy storage system integrated with a cascaded latent heat cold thermal energy storage. *Energy* 2023;281:128203. <https://doi.org/10.1016/J.ENERGY.2023.128203>.
- [19] Qu Y, Lin X, Wang L, Zhang S, Bai Y, Ge Z, et al. Cryogenic energy storage characteristics in cascaded packed beds. *J Energy Storage* 2023;73. <https://doi.org/10.1016/j.est.2023.108867>.
- [20] She X, Wang X, Han P, Li Y, Wang C. Enhancement of efficiencies of cryogenic energy storage packed bed using a novel Referred-Standard-Volume optimization method. *Int J Heat Mass Transf* 2024;224:125367. <https://doi.org/10.1016/J.IJHEATMASSTRANSFER.2024.125367>.
- [21] Dumont O, Frate GF, Pillai A, Lecompte S, De paepe M, Lemort V. Carnot battery technology: A state-of-the-art review. *J Energy Storage* 2020;32. <https://doi.org/10.1016/j.est.2020.101756>.
- [22] Lee I, Park J, Moon I. Conceptual design and exergy analysis of combined cryogenic energy storage and LNG regasification processes: Cold and power integration. *Energy* 2017;140:106–15. <https://doi.org/10.1016/j.energy.2017.08.054>.
- [23] She X, Zhang T, Cong L, Peng X, Li C, Luo Y, et al. Flexible integration of liquid air energy storage with liquefied natural gas regasification for power generation enhancement. *Appl Energy* 2019;251:113355. <https://doi.org/10.1016/j.apenergy.2019.113355>.
- [24] Peng X, She X, Li C, Luo Y, Zhang T, Li Y, et al. Liquid air energy storage flexibly coupled with LNG regasification for improving air liquefaction. *Appl Energy* 2019;250:1190–201. <https://doi.org/10.1016/j.apenergy.2019.05.040>.
- [25] Park J, Lee I, Moon I. A Novel Design of Liquefied Natural Gas (LNG) Regasification Power Plant Integrated with Cryogenic Energy Storage System. *Ind Eng Chem Res* 2017;56:1288–96. <https://doi.org/10.1021/acs.iecr.6b04157>.
- [26] Park J, Cho S, Qi M, Noh W, Lee I, Moon I. Liquid air energy storage coupled with liquefied natural gas cold energy: Focus on efficiency, energy capacity, and flexibility. *Energy* 2021;216:119308. <https://doi.org/10.1016/J.ENERGY.2020.119308>.
- [27] Kim Y, Qi M, Cho J, Lee I, Park J, Moon I. Process design and analysis for combined hydrogen regasification process and liquid air energy storage. *Energy* 2023;283:129093. <https://doi.org/10.1016/J.ENERGY.2023.129093>.
- [28] Hydrogen n.d. [https://energy.ec.europa.eu/topics/energy-systems-integration/hydrogen\\_en](https://energy.ec.europa.eu/topics/energy-systems-integration/hydrogen_en) (accessed August 22, 2024).
- [29] Energy Market Authority (EMA). Charting the energy transition to 2050 - Energy 2050 Committee report 2022.
- [30] IRENA (International Renewable Energy Agency). Global hydrogen trade to meet the 1.5 °C climate goal: Part II – Technology review of hydrogen carriers. *Global Hydrogen Trade to Meet the 15°C Climate Goal: Technology Review of Hydrogen Carriers* 2022.
- [31] Keppel breaks ground on 600MW Singapore gas power plant n.d. <https://www.power-technology.com/news/keppel-break-ground-power-plant/> (accessed August 16, 2024).

- [32] Hank C, Sternberg A, Köppel N, Holst M, Smolinka T, Schaadt A, et al. Energy efficiency and economic assessment of imported energy carriers based on renewable electricity. *Sustain Energy Fuels* 2020;4:2256–73. <https://doi.org/10.1039/d0se00067a>.
- [33] Restelli F, Spatolisano E, Pellegrini LA, Cattaneo S, de Angelis AR, Lainati A, et al. Liquefied hydrogen value chain: A detailed techno-economic evaluation for its application in the industrial and mobility sectors. *Int J Hydrogen Energy* 2024;52:454–66. <https://doi.org/10.1016/J.IJHYDENE.2023.10.107>.
- [34] Hu SC, Lin T, Huang SH, Fu BR, Hu MH. Energy savings approaches for high-tech manufacturing factories. *Case Studies in Thermal Engineering* 2020;17:100569. <https://doi.org/10.1016/J.CSITE.2019.100569>.
- [35] Wang C, Zhang X, You Z, Zhang M, Huang S, She X. The effect of air purification on liquid air energy storage – An analysis from molecular to systematic modelling. *Appl Energy* 2021;300:117349. <https://doi.org/10.1016/J.APENERGY.2021.117349>.
- [36] The Centre for Low Carbon Futures. Liquid Air in the energy and transport systems. 2013.
- [37] Borri E, Tafone A, Romagnoli A, Comodi G. A preliminary study on the optimal configuration and operating range of a “microgrid scale” air liquefaction plant for Liquid Air Energy Storage. *Energy Convers Manag* 2017;143:275–85. <https://doi.org/10.1016/j.enconman.2017.03.079>.
- [38] Tafone A, Romagnoli A, Borri E, Comodi G. New parametric performance maps for a novel sizing and selection methodology of a Liquid Air Energy Storage system. *Appl Energy* 2019;250:1641–56. <https://doi.org/10.1016/j.apenergy.2019.04.171>.
- [39] Tafone A, Borri E, Comodi G, Broek M Van Den. Liquid Air Energy Storage performance enhancement by means of Organic Rankine Cycle and Absorption Chiller. *Appl Energy* 2018;228:1810–21. <https://doi.org/10.1016/j.apenergy.2018.06.133>.
- [40] Pili R, Spliethoff H. Design and Off-Design of Organic Rankine Cycle Systems Recovering Fluctuating Industrial Waste Heat n.d.
- [41] Tafone A, Pili R, Pihl Andersen M, Romagnoli A. Dynamic modelling of a compressed heat energy storage (CHEST) system integrated with a cascaded phase change materials thermal energy storage. *Appl Therm Eng* 2023;226:120256. <https://doi.org/10.1016/J.APPLTHERMALENG.2023.120256>.
- [42] Keppel to develop Singapore’s first hydrogen-ready power plant, with construction undertaken by Mitsubishi Power Asia Pacific and Jurong Engineering consortium - Keppel Infrastructure n.d. <https://www.keppinfra.com/en/news-item.aspx?aid=16124&title=keppel-to-develop-singapores-first-hydrogen-ready-power-plant> (accessed September 12, 2023).
- [43] Bell I, Quoillin S, Wronski J, Lemort V. Coolprop: An open-source referencequality thermophysical property library. Submitted Abstract to ASME- ... 2013:110006.
- [44] Bell IH, Wronski J, Quoillin S, Lemort V. Pure and pseudo-pure fluid thermophysical property evaluation and the open-source thermophysical property library coolprop. *Ind Eng Chem Res* 2014;53:2498–508. [https://doi.org/10.1021/IE4033999/SUPPL\\_FILE/IE4033999\\_SI\\_002.ZIP](https://doi.org/10.1021/IE4033999/SUPPL_FILE/IE4033999_SI_002.ZIP).
- [45] Son H, Yu T, Hwang J, Lim Y. Simulation methodology for hydrogen liquefaction process design considering hydrogen characteristics. *Int J Hydrogen Energy* 2022;47:25662–78. <https://doi.org/10.1016/J.IJHYDENE.2022.05.293>.
- [46] Thermophysical Properties of Fluid Systems n.d. <https://webbook.nist.gov/chemistry/fluid/> (accessed May 2, 2025).
- [47] Lemmon EW, Jacobsen RT, Penoncello SG, Friend DG. Thermodynamic properties of air and mixtures of nitrogen, argon, and oxygen from 60 to 2000 K at pressures to 2000 MPa. *J Phys Chem Ref Data* 2000;29:331–62. <https://doi.org/10.1063/1.1285884>.

- [48] Wilson DG, Korakianitis T. The Design of High-Efficiency Turbomachinery and Gas Turbines. *The Design of High-Efficiency Turbomachinery and Gas Turbines* 2014. <https://doi.org/10.7551/MITPRESS/9940.001.0001>.
- [49] Chang HM, Lim HS, Choe KH. Effect of multi-stream heat exchanger on performance of natural gas liquefaction with mixed refrigerant. *Cryogenics (Guildf)* 2012;52:642–7. <https://doi.org/10.1016/j.cryogenics.2012.05.014>.
- [50] Tafone A, Borri E, Cabeza LF, Romagnoli A. Innovative cryogenic Phase Change Material (PCM) based cold thermal energy storage for Liquid Air Energy Storage (LAES) – Numerical dynamic modelling and experimental study of a packed bed unit. *Appl Energy* 2021;301:117417. <https://doi.org/10.1016/J.APENERGY.2021.117417>.
- [51] Pili R, Romagnoli A, Jiménez-Arreola M, Spliethoff H, Wieland C. Simulation of Organic Rankine Cycle – Quasi-steady state vs dynamic approach for optimal economic performance. *Energy* 2019;167:619–40. <https://doi.org/10.1016/J.ENERGY.2018.10.166>.
- [52] Pili R, Spliethoff H. Design and Off-Design of Organic Rankine Cycle Systems Recovering Fluctuating Industrial Waste Heat n.d.
- [53] Tafone A, Pili R, Pihl Andersen M, Romagnoli A. Dynamic modelling of a compressed heat energy storage (CHEST) system integrated with a cascaded phase change materials thermal energy storage. *Appl Therm Eng* 2023;226:120256. <https://doi.org/10.1016/J.APPLTHERMALENG.2023.120256>.
- [54] Organic Rankine Cycle (ORC) Power Systems. *Organic Rankine Cycle (ORC) Power Systems* 2017. <https://doi.org/10.1016/C2014-0-04239-6>.
- [55] Pili R, Bojer Jørgensen S, Haglind F. Multi-objective optimization of organic Rankine cycle systems considering their dynamic performance. *Energy* 2022;246:123345. <https://doi.org/10.1016/J.ENERGY.2022.123345>.
- [56] Richard Turton, Richard C. Bailie, Wallace B. Whiting JAS. *Analysis, Synthesis and Design of Chemical Processes Third Edition*. vol. 53. 2013. <https://doi.org/10.1017/CBO9781107415324.004>.
- [57] Seider WD, Lewin DR, Seader JD, Widagdo S, Gani R, Ng KM. *Product and process design principles*. Fourth edi. New York: Wiley; 2017.
- [58] Couper JR, Penney WRoy, Fair JR, Walas SM. *Chemical process equipment: selection and design*. Rev. 2nd e. London: Elsevier Butterworth-Heinemann; 2009. <https://doi.org/https://doi.org/10.1016/C2011-0-08248-0>.
- [59] Schoen HM. *Plant Design and Economics for Chemical Engineers*. Max S. Peters. McGraw-Hill, New, York, 1958. xi+ 511 pp. Illus. \$11. *Science* (1979) 1958;128:1000–1000. <https://doi.org/10.1126/SCIENCE.128.3330.1000.B>.
- [60] Hewitt GF, Pugh SJ. Approximate Design and Costing Methods for Heat Exchangers. *Heat Transfer Engineering* 2007;28:76–86. <https://doi.org/10.1080/01457630601023229>.
- [61] Jülch V. Comparison of electricity storage options using levelized cost of storage (LCOS) method. *Appl Energy* 2016;183:1594–606. <https://doi.org/10.1016/j.apenergy.2016.08.165>.
- [62] Electricity Tariff Revision For The Period 1 April to 30 June 2023 n.d. <https://www.spgroup.com.sg/about-us/media-resources/news-and-media-releases/Electricity-Tariff-Revision-For-The-Period-1-April-to-30-June-2023> (accessed February 5, 2024).
- [63] Tafone A, Ding Y, Li Y, Xie C, Romagnoli A. Levelised Cost of Storage (LCOS) analysis of liquid air energy storage system integrated with Organic Rankine Cycle. *Energy* 2020;198:117275. <https://doi.org/10.1016/j.energy.2020.117275>.

- [64] Tafone A, Ding Y, Li Y, Xie C, Romagnoli A. Levelised Cost of Storage (LCOS) analysis of liquid air energy storage system integrated with Organic Rankine Cycle. *Energy* 2020;198:117275. <https://doi.org/10.1016/j.energy.2020.117275>.
- [65] Hu SC, Lin T, Huang SH, Fu BR, Hu MH. Energy savings approaches for high-tech manufacturing factories. *Case Studies in Thermal Engineering* 2020;17:100569. <https://doi.org/10.1016/j.csite.2019.100569>.
- [66] Maxwell C. Cost Indices n.d.
- [67] Xiao F, Yang L, He L, Gil A, Rajoo S, Zhao Z, et al. Performance enhancement of horizontal extension and thermal energy storage to an abandoned exploitation well and satellite LNG station integrated ORC system. *Appl Therm Eng* 2022;214:118736. <https://doi.org/10.1016/j.applthermaleng.2022.118736>.
- [68] She X, Peng X, Nie B, Leng G, Zhang X, Weng L, et al. Enhancement of round trip efficiency of liquid air energy storage through effective utilization of heat of compression. *Appl Energy* 2017;206:1632–42. <https://doi.org/10.1016/j.apenergy.2017.09.102>.
- [69] Schmidt O, Staffell I. Monetizing Energy Storage: A Toolkit to Assess Future Cost and Value. *Monetizing Energy Storage: A Toolkit to Assess Future Cost and Value* 2023:1–330. <https://doi.org/10.1093/OSO/9780192888174.001.0001>.
- [70] Georgiou S, Shah N, Markides CN. A thermo-economic analysis and comparison of pumped-thermal and liquid-air electricity storage systems. *Appl Energy* 2018;226:1119–33. <https://doi.org/10.1016/j.apenergy.2018.04.128>.
- [71] Li D, Duan L. Techno-economic analysis of solar aided liquid air energy storage system with a new air compression heat utilization method. *Energy Convers Manag* 2023;278:116729. <https://doi.org/10.1016/J.ENCONMAN.2023.116729>.
- [72] Park JH, Heo JY, Lee JI. Techno-economic study of nuclear integrated liquid air energy storage system. *Energy Convers Manag* 2022;251:114937. <https://doi.org/10.1016/J.ENCONMAN.2021.114937>.
- [73] Lin B, Wu W, Bai M, Xie C. Liquid air energy storage: Price arbitrage operations and sizing optimization in the GB real-time electricity market. *Energy Econ* 2019;78:647–55. <https://doi.org/10.1016/j.eneco.2018.11.035>.
- [74] Xie C, Li Y, Ding Y, Radcliffe J. ScienceDirect Evaluating Levelized Cost of Storage ( LCOS ) Based on Price Arbitrage Operations : with Liquid Air Energy Storage ( LAES ) as an Example 2018;00:22–5.
- [75] Xie C, Hong Y, Ding Y, Li Y, Radcliffe J. An economic feasibility assessment of decoupled energy storage in the UK: With liquid air energy storage as a case study. *Appl Energy* 2018;225:244–57. <https://doi.org/10.1016/j.apenergy.2018.04.074>.
- [76] Vecchi A, Naughton J, Li Y, Mancarella P, Sciacovelli A. Multi-mode operation of a Liquid Air Energy Storage (LAES) plant providing energy arbitrage and reserve services – Analysis of optimal scheduling and sizing through MILP modelling with integrated thermodynamic performance. *Energy* 2020;200:117500. <https://doi.org/10.1016/j.energy.2020.117500>.